

15_039_1
FHR reports

Investigation into the non-linear hydrodynamical processes in the Scheldt River

Idealised processes study

Investigation into the non-linear hydrodynamical processes in the Scheldt River

Idealised processes study

Dijkstra, Y.M.

Legal notice

Flanders Hydraulics Research is of the opinion that the information and positions in this report are substantiated by the available data and knowledge at the time of writing.

The positions taken in this report are those of Flanders Hydraulics Research and do not reflect necessarily the opinion of the Government of Flanders or any of its institutions.

Flanders Hydraulics Research nor any person or company acting on behalf of Flanders Hydraulics Research is responsible for any loss or damage arising from the use of the information in this report.

Copyright and citation

© The Government of Flanders, Department of Mobility and Public Works, Flanders Hydraulics Research, 2022
D/2022/3241/188

This publication should be cited as follows:

Dijkstra, Y.M. (2022). Investigation into the non-linear hydrodynamical processes in the Scheldt River: Idealised processes study. Version 4.0. FHR Reports, 15_039_1. Flanders Hydraulics Research: Antwerp

Reproduction of and reference to this publication is authorised provided the source is acknowledged correctly.

Document identification

Customer:	Flemish-Dutch Scheldt Committee	Ref.:	WL2022R15_039_1
Keywords (3-5):	Estuaries, Scheldt, tides, hydraulic roughness		
Knowledge domains:	Hydrodynamics > Tides > Numerical modelling Hydrodynamics > Current velocities and patterns > Numerical modelling Hydrodynamics > Water levels > Numerical modelling Hydrodynamics > Turbulence > Numerical modelling		
Text (p.):	25	Appendices (p.):	9
Confidential:	No	<input checked="" type="checkbox"/> Available online	
Author(s):	Dijkstra, Y. M.		

Control

	Name	Signature
Revisor(s):	Schuttelaars, H. M.	Henk Schuttelaars Digitally signed by Henk Schuttelaars Date: 2022.11.23 09:42:26 +01'00'
Project leader:	Schramkowski, G. P.	Dr. George P. Schramkowski Digitaal ondertekend door Dr. George P. Schramkowski Datum: 2022.12.01 11:11:46 +01'00'

Approval

Head of division:	Bellafkih, A.	Getekend door: Abdelkarim Bellafkih (Sign) Getekend op: 2022-12-01 11:35:28 +01:0 Redelijk keur dit document goed <i>Abdelkarim Bellafkih</i>
-------------------	---------------	--



Abstract

This study presents an investigation into the non-linear hydrodynamics in the Scheldt River estuary using the two-dimensional vertical (2DV) idealised iFlow model. It extends the earlier study by Brouwer *et al.* (2017) on weakly non-linear hydrodynamics by including higher-order non-linear physical mechanisms and non-linear parametrisations of turbulent mixing. The goals of this study are to a) simplify the calibration of the model, by reducing the number of calibration parameters from two to one, (b) improve the performance of the idealised iFlow model in the Upper Sea Scheldt and (c) understand the essential physical mechanisms required for such improved performance.

The $k - \epsilon$ turbulence closure model was used to derive linear and non-linear parametrisations of turbulence that depend only on one calibration parameter. The calibration yields a clear best fit for the M_2 tide, while no single best value for the M_4 tide could be found. The result of the calibration on the M_2 tide yields a good description of this tidal component, though the amplitude is overestimated in the Upper Sea Scheldt when using the linear model. The M_4 tidal amplitude is typically overestimated by the model in the whole estuary. The relative phase of both the M_2 and M_4 tidal components are well described.

The higher-order non-linear mechanisms are insignificant for the Western Scheldt and Lower Sea Scheldt, but are important in the Upper Sea Scheldt. The model shows a further set-up of the M_2 tide in the Upper Sea Scheldt as a consequence of these mechanisms. This set-up increases the discrepancy between modelled and measured water levels. Damping of the M_2 tide is achieved by including a non-linear description of turbulent mixing. This description relates turbulent mixing to the local velocity magnitude. The relatively high tidal velocity in the Upper Sea Scheldt then produces additional mixing and therefore damping of the tide. An additional source of damping is found by including time variations of turbulent mixing on the tidal time-scale. This also improves the correspondence between the modelled and measured M_4 tide. Nevertheless, the error in the modelled M_4 tidal amplitude remains large, with values up to 100%. The total effect of all non-linear terms and turbulent mixing improve the result compared to that of Brouwer *et al.* (2017), but do nevertheless not produce a sufficient degree of damping of the tide in the Upper Sea Scheldt. It is therefore concluded that a change in the roughness value or the representative depth of the system is required to further improve the model result.

The additional physical mechanisms studied in this report do not lead to a qualitative change in measures of tidal asymmetry. Although these measures provide an indication for the direction of the net sediment transport, the effect of non-linear terms on the net sediment transport remains to be investigated.

Contents

Abstract.....	III
List of Figures	VI
List of Tables	VII
1 Introduction	1
2 Model	2
2.1 Scheldt base model	2
2.2 Modelling method.....	3
2.3 Formulations for the eddy viscosity and bottom friction	6
2.3.1 Linear single parameter formulation	6
2.3.2 Non-linear scaled formulation	6
2.3.3 Non-linear truncated formulation	7
3 Results.....	9
3.1 Base model.....	9
3.1.1 Base model of Brouwer <i>et al.</i> (2017)	9
3.1.2 Linear single-parameter calibration	10
3.2 Higher-order dynamics	12
3.2.1 Higher-order water levels.....	12
3.2.2 Decomposition of the second-order dynamics	13
3.2.3 Tide-river interaction.....	13
3.3 Non-linear bottom friction	16
3.3.1 Constant eddy viscosity	16
3.3.2 Time-dependent eddy viscosity.....	17
3.4 Consequences for tidal asymmetry	21
4 Conclusions	23
References	25
A1 About the iFlow modelling framework	A1
A2 Model equations	A2
A2.1 Hydrodynamics	A2
A2.1.1 Leading-order and first-order model	A2
A2.1.2 Higher-order model	A5
A2.2 Derivation of the turbulence closures	A6
A2.2.1 M_2 tidal forcing and constant subtidal eddy viscosity	A7
A2.2.2 Arbitrary forcing and time-varying eddy viscosity	A8

List of Figures

Figure 1	Map of the Scheldt River estuary from Brouwer <i>et al.</i> (2017).	2
Figure 2	Smooth fitting of the width and depth (red lines) to the measured width and depth in 2013.	3
Figure 3	Sketch of a typical width (a) and depth (b) profile in the model.	4
Figure 4	Schematic overview of the physical mechanisms affecting the flow and their interaction with the turbulence model.	7
Figure 5	Schematic overview of the truncated turbulence model approach.	8
Figure 6	Plot of the cost function that compares the fit between the measurements and model result for the M_2 tide (a) and M_4 tide (b).	9
Figure 7	Model results of the base model (solid lines) compared to measurements (dots) for the water level amplitude (a), water level phase (b) and depth-averaged velocity amplitude (c) along the Scheldt River.	10
Figure 8	Cost function for the M_2 tide (a) and M_4 tide (b) as a function of the calibration parameter s_f	11
Figure 9	Model results of the linear single-parameter model (solid lines) compared to measurements (dots) for the water level amplitude (a) and water level phase (b) along the Scheldt River.	11
Figure 10	Model results of the higher-order linear single-parameter model (solid lines) compared to the first-order model (dashed lines) and to measurements (dots) for the water level amplitude (a) and water level phase (b) along the Scheldt River.	12
Figure 11	Physical mechanism contributing to the second-order water level amplitude.	14
Figure 12	Eddy viscosity, eddy viscosity scaled by the depth and roughness parameter s_f along the length of the estuary.	14
Figure 13	Computed water level amplitude for typical summer ($Q = 20 \text{ m}^3/\text{s}$) and winter ($Q = 70 \text{ m}^3/\text{s}$) conditions up to the sixth order.	15
Figure 14	Cost function for the M_2 tide (a) and M_4 tide (b) up to sixth order as a function of the calibration parameter $z_0^* = z_0/H$	16
Figure 15	Eddy viscosity, eddy viscosity scaled by the depth and partial slip parameter s_f along the length of the estuary.	17
Figure 16	Model results of the non-linear model at first order (dashed lines) and sixth order (solid lines) compared to measurements (dots) for the water level amplitude (a), water level phase (b) and depth-averaged velocity amplitude (c) along the Scheldt River.	18
Figure 17	Eddy viscosity, eddy viscosity scaled by the depth and roughness parameter s_f along the length of the estuary.	19
Figure 18	Model results of the non-linear model with time-varying eddy viscosity at first order (dashed lines) and sixth order (solid lines) compared to measurements (dots) for the water level amplitude (a), water level phase (b) and depth-averaged velocity amplitude (c) along the Scheldt River.	20
Figure 19	Two measures for the tidal asymmetry for four different model configurations.	22
Figure 20	Quality of fit for relation (A-7) (left) and (A-8) (right).	A7
Figure 21	Fitting of the sub-tidal part of $f_0(\alpha) = A_\nu/U_{M_2}$ and $g_0(\beta) = A_\nu/U_{M_2}$ as function of $\alpha = U_{\text{sub-tidal}}/U_{M_2}$ and $\beta = U_{M_4}/U_{M_2}$	A9
Figure 22	Fitting of $A_{\nu M_2}/A_{\nu \text{sub-tidal}}$ (green) and $A_{\nu M_4}/A_{\nu \text{sub-tidal}}$ (red) as function of $\alpha = U_{\text{sub-tidal}}/U_{M_2}$ and $\beta = U_{M_4}/U_{M_2}$	A9

List of Tables

Table 1	Stations of water level measurements	4
Table 2	Overview of the physical mechanisms acting on the flow and the order where they appear in the equations.....	5

1 Introduction

This report presents the results of a study into the effects of non-linear interactions on the tidal propagation in the Scheldt River estuary. This study is part of the PhD project 'Regimes shifts in tidal estuaries' at TU Delft and Deltares. The goal of the full program is to assess whether the Scheldt River might possibly develop into a hyper-turbid estuary. This study involves developing and using an idealised model. This model is especially suited for gaining an understanding of the physical processes involved and testing the robustness of these mechanisms to different scenarios. It is also well suited for doing sensitivity studies to cover the uncertainty in the values of model parameters.

This study extends the hydrodynamic model by Brouwer *et al.* (2017) (WL project 13_103, part 1.3). The base model contains two calibration parameters: the eddy viscosity A_ν and the partial-slip roughness parameter s_f , which have been calibrated for the Scheldt River. It was identified that there exists a wide band of the calibration parameters with similarly accurate model results, leading to a degree of arbitrariness in the values of these parameters. One of the goals for this study is to reduce the two calibration parameters to a single parameter with a single best value.

It was also found by Brouwer *et al.* (2017) that the measured M_2 and M_4 tidal surface elevations in the Upper-Sea Scheldt could not be well reproduced by the base model. One of the identified potential reasons is the solution method. This method assumes that the solution, for example the water level ζ , can be written as a series $\zeta^0 + \zeta^1 + \dots$, where each of the terms ζ^i ($i = 0, 1, \dots$) are easier to solve for than the full solution. Furthermore, every subsequent term ζ^{n+1} is typically around a factor ϵ smaller than the previous term ζ^n , where ϵ is defined as the variation of the surface level divided by the depth. Typically ϵ is much smaller than unity in the Scheldt River, so that just the combination of ζ^0 and ζ^1 already yield an accurate approximation of the full solution. These terms are therefore the only terms taken into account by Brouwer *et al.* (2017). However, ϵ is not small in the Upper Sea Scheldt, so that ζ^2 , ζ^3 and other higher-order terms are potentially important. The second goal of this study is to identify whether these terms are indeed important to the accurate assessment of the water levels in the Upper Sea Scheldt.

Finally, not only the higher-order solutions, but also the turbulence model used can have an important effect on the model solution throughout the Scheldt River. We will therefore test a turbulence closure that relates the eddy viscosity to the local depth and velocity.

The model will be briefly discussed in Chapter 2, refraining from the model equations and details, which are provided in Appendix A2. Chapter 3 then discusses the results, starting with the base model and then showing the effect of the individual model extensions discussed above. The conclusions are finally presented in Chapter 4.

2 Model

The model used for this study is the 2DV idealised process-based model iFlow (Dijkstra *et al.*, 2017b), which was used to study the hydrodynamics in the Scheldt River by Brouwer *et al.* (2017). Here, we use a numerical variant of the same model, which allows making several extensions to solve for more non-linear processes than were included by Brouwer *et al.* (2017). Section 2.1 discusses the Parametrisation of the geometry and forcing of the Scheldt River. Next, 2.2 provides a short overview of the hydrodynamical model and the method used for the decomposition of physical components. Section 2.3 finally presents several alternative linear and non-linear turbulence closures.

2.1 Scheldt base model

The 2DV model for the Scheldt River developed by Brouwer *et al.* (2017) is the starting point for this study. In this model, the length of the estuary is approximately 160 km, measured from Vlissingen to the tidal weirs and locks in Gentbrugge, which mark the end of the tidal river. The base model assumes a single-channel system, without bifurcations en confluences. This implies that the Ruppel tributary is not explicitly taken into account. Similarly, the two branches in Gentbrugge and various smaller sluices and locks connecting to the Scheldt are not explicitly modelled, see also Figure 1. The width and depth of the estuary in the model are given by smooth function fits to the measured depth and width of 2013, see Figure 2.

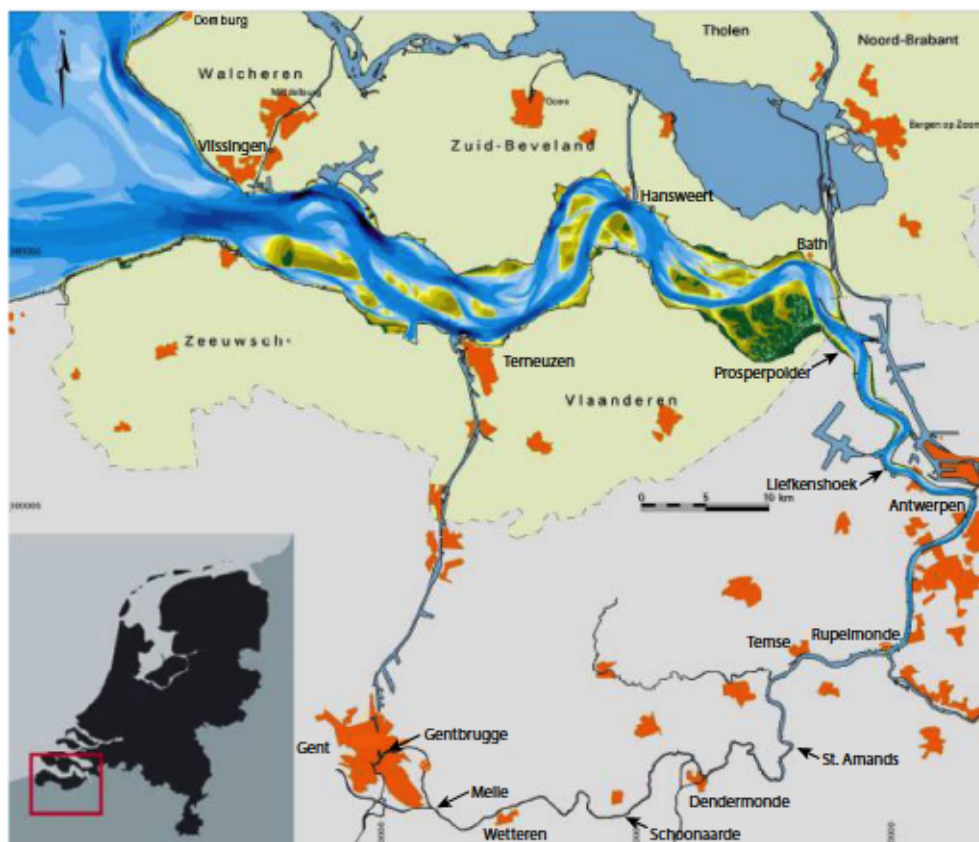


Figure 1 – Map of the Scheldt River estuary from Brouwer *et al.* (2017). Note that the Scheldt River has several bifurcations and confluences that are not explicitly modelled.

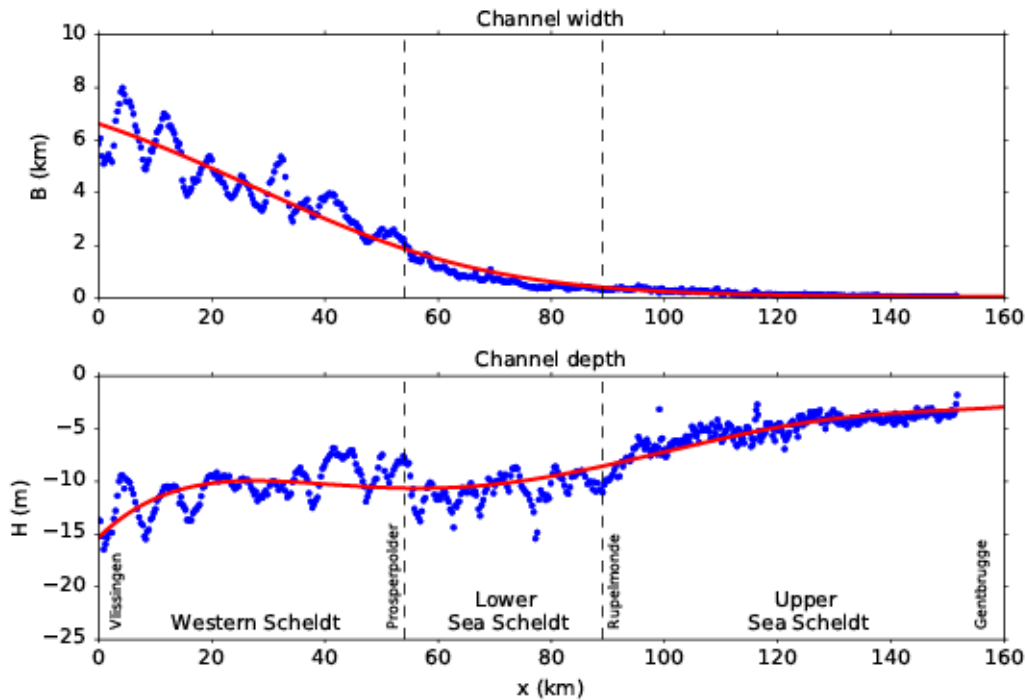


Figure 2 – Smooth fitting of the width and depth (red lines) to the measured width and depth in 2013. From Brouwer *et al.* (2017).

The water motion is forced by a prescribed sea surface elevation at Vlissingen that consists the average observed M_2 and M_4 tidal water level amplitudes. The average M_2 amplitude equals 1.77 m, the M_4 amplitude equals 0.14 m with a relative phase of -1.3 degrees. Additional to the sea surface elevation at Vlissingen, the water motion is forced by a river discharge at the tidal weir. This discharge is assumed constant at a typical summer value of $20 \text{ m}^3/\text{s}$. The typical along-channel subtidal salinity profile for summer conditions has been derived from measurements and is described by a smoothly decreasing function that is approximately zero at 100 km into the estuary. Vertical or temporal variations in the salinity profile are small within the course of a season and are therefore not taken into account.

Water level measurements based on time series measured at 13 stations along the estuary in 2009 are used to calibrate and validate the model results. The stations and their distance from Vlissingen are listed in Table 1. Measurements of the subtidal, M_2 and M_4 velocity are obtained from measurement campaigns at 11 stations along the estuary between 2011 and 2014. The measurements as presented here are the along-channel velocities based on ADCP measurements along cross-sectional transects. More information on the measurements can be found in Brouwer *et al.* (2017).

2.2 Modelling method

The model is based on the tidal river model by Ianniello (1977, 1979) and Chernetsky *et al.* (2010) and solves for the width-averaged tidal elevation ζ , width-averaged horizontal flow velocity u and width-averaged vertical flow velocity w . The model domain is sketched in Figure 3. The width B and depth H are allowed to vary arbitrarily but smoothly in the along-channel direction. The length of the tidal river is bounded, with the mouth of the river at $x = 0$ and a tidal weir at $x = L$. The variation of the horizontal and vertical velocity is resolved over the vertical direction z between the bed $z = -H$ and the mean sea level at $z = 0$.

The equations for tidal flows are non-linear, which renders them generally hard to solve. The equations can be strongly simplified using a *perturbation method*. The method used here assumes that the water level elevation

Table 1 – Stations of water level measurements

Station	Distance to Vlissingen (km)
Vlissingen	0
Terneuzen	18.5
Hansweert	33.8
Bath	49.8
Prosperpolder	54
Liefkenshoek	61.1
Antwerpen	75.6
Temse	97.3
St. Amands	106.8
Dendermonde	119.8
Schoonaarde	130.6
Wetteren	142.7
Melle	148.8

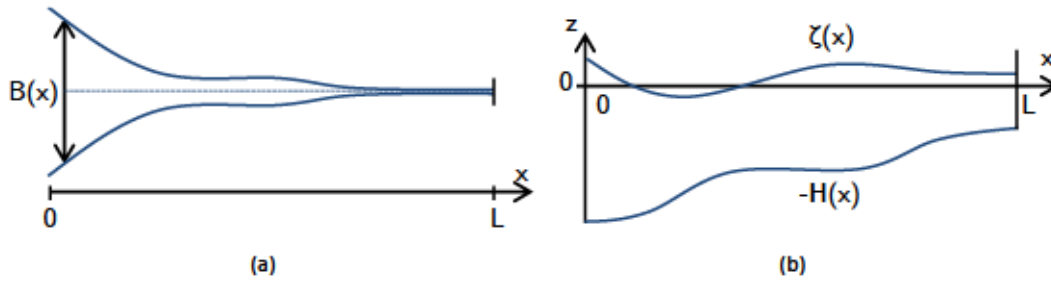


Figure 3 – Sketch of a typical width (a) and depth (b) profile in the model.

ζ is small compared to the depth. This condition is formally expressed as

$$\epsilon = \left. \frac{\zeta}{H} \right|_{x=0} \ll 1.$$

Consequently, the water level, velocity components and eddy viscosity is written as a series

$$\begin{aligned} \zeta &= \zeta^0 + \zeta^1 + \zeta^2 + \dots, \\ u &= u^0 + u^1 + u^2 + \dots, \\ w &= w^0 + w^1 + w^2 + \dots, \\ A_\nu &= A_\nu^0 + A_\nu^1 + A_\nu^2 + \dots, \end{aligned}$$

where the super-scripts denote the order (0=leading order, 1=first order etc.). It is assumed that ζ^1 is typically a factor ϵ smaller than ζ^0 , ζ^2 is a factor ϵ smaller than ζ^1 etcetera. It follows that the orders of ζ quickly become smaller if ϵ is sufficiently small.

It is assumed that the externally generated M_4 tidal amplitude is of order ϵ (i.e. small) compared to the M_2 tide and that the river discharge velocity is of order ϵ compared to the typical M_2 tidal velocity. The latter assumption is technically not valid near the tidal weir, where the river velocity is larger than the vanishing tidal velocity. In practice this is however not a problem, as the model still resolves the river flow reasonably well. Furthermore it is assumed that the salinity field is well mixed and stationary and that the effect of wind, waves, river bends, side channels and tidal flats on the tidal flow are negligible.

Under the above assumptions, it is found by a scaling analysis that all non-linear terms in the equations of motion are of order ϵ compared to the linear terms. As a consequence, the full non-linear equations are approximated up to leading order by a linear estimate of the leading-order M_2 tidal flow. The first-order

correction contains a linear estimate of the M_4 tidal and constant river flows and a linear estimate of the non-linearities acting on the M_2 tidal flow. Even higher orders contain linear estimates of the non-linear terms acting on the M_4 tidal and river flows and non-linear interactions between the tidal and river components. The linear equations at each order are easily solved for and provide insight into the physical mechanisms that act on the flow. The physical mechanisms distinguished by the model are listed in Table 2 together with a short description and the order at which each mechanism appears.

Table 2 – Overview of the physical mechanisms acting on the flow and the order where they appear in the equations.

Mechanism	Description	Order
External tide	Linear propagation of the M_2 (leading order) and M_4 (first order) tide forced from the North Sea	0, 1
River	Constant river discharge	1
Baroclinic	Flow generated by the baroclinic pressure, caused by the horizontal salinity gradient	1
Advection	Non-linear effect of tidal propagation due to spatial acceleration or deceleration of the flow	≥ 1
No-stress correction	Non-linear effect of tidal propagation originating from momentum of the flow generated between the actual surface and the reference surface ($z = 0$)	≥ 1
Tidal return flow	Non-linear effect of tidal propagation originating from the correlation between the velocity and water level elevation (also known as Stokes drift). This correlation leads to a transport of water that needs to be compensated by a return flow in order to satisfy the balance of mass	≥ 1
Mixing correction	Flow correction by modelled corrections to the level of turbulent mixing made at the same order. This only applies if the eddy viscosity is made dependent on the water level or velocity	≥ 1

The total computed surface elevation and velocity consist of the externally forced M_2 , M_4 and subtidal components as well as over-tides (M_4 , M_6 , M_8 etc.) generated by non-linear interactions. In practice, it is sufficiently accurate to describe the total surface elevation and velocity by a finite number of over-tide components. This allows us to express the solution as

$$\begin{aligned}
 \zeta &= \Re \left(\sum_{n=0}^{f_{\max}} \hat{\zeta}_n e^{n\omega t} \right), \\
 u &= \Re \left(\sum_{n=0}^{f_{\max}} \hat{u}_n e^{n\omega t} \right), \\
 w &= \Re \left(\sum_{n=0}^{f_{\max}} \hat{w}_n e^{n\omega t} \right).
 \end{aligned} \tag{1}$$

Here, ω is the angular frequency of the M_2 tide and the variables $\hat{\zeta}_n$, \hat{u}_n and \hat{w}_n contain the amplitude and phase information of the tidal component M_{2n} . In our study $f_{\max} = 5$, which means that the model resolves all tidal components up to the M_{10} tide. This *harmonic decomposition* means that the model does not need any time-integration method, but can solve for the tidal components directly.

2.3 Formulations for the eddy viscosity and bottom friction

In the model of Brouwer *et al.* (2017), the effects of friction are governed by the vertical eddy viscosity A_ν and partial-slip parameter s_f . These parameters are assumed constant along the estuary. Most complex three-dimensional models however use the $k - \epsilon$ turbulence closure model to calculate a vertical eddy viscosity coefficient that varies in time and space according to a non-linear partial differential equation that depends on the velocity and depth. Such models additionally often use quadratic slip boundary conditions. The $k - \epsilon$ model uses only one calibration parameter, which is the bed roughness z_0 .

In order to capture some of the complex spatial and temporal behaviour of the eddy viscosity, we parametrise it using a set of new, relatively simple linear and non-linear turbulence closures that are derived from the $k - \epsilon$ model. To this end, the $k - \epsilon$ model has been run in a water column model for 400 experiments with different tidal flows and varying values for the velocity, depth and roughness. Vertically uniform eddy viscosity profiles have been fitted to each of these experiments, so that one obtains closures that relate the eddy viscosity A_ν and partial slip parameter s_f to the velocity u , depth H and bed roughness z_0 . The fitting procedure is discussed in more detail in Appendix A2.

2.3.1 Linear single parameter formulation

The first relation obtained from fitting the eddy viscosity to the $k - \epsilon$ model is

$$A_\nu = 0.5s_f H. \quad (2)$$

This relation states that there is a fixed relation between A_ν and s_f in tidal flows that only depends on the local depth. This relation does not depend on the velocity, so that the hydrodynamic model remains linear. It is thus a fast and easy method for reducing the two calibration parameters A_ν and s_f to a single calibration parameter s_f .

2.3.2 Non-linear scaled formulation

Alternatively one can use the dimensionless roughness height z_0^* as calibration parameter. This parameter represents the size of 'roughness-determining elements', such as ripples and dunes on the bed, relative to the local depth. This is arguably a more correct roughness parameter than s_f , because s_f follows from a Lorentz linearisation, which means it is a combination of the roughness and a typical near-bed velocity. Using the result of the $k - \epsilon$ model for tidal flows, both A_ν and s_f can be related to z_0^* according to

$$A_\nu = 0.16|u|H \left((1 + z_0^*) \ln \left(\frac{1}{z_0^*} + 1 \right) - 1 \right)^{-2}, \quad (3)$$

$$s_f = 0.35|u| \left((1 + z_0^*) \ln \left(\frac{1}{z_0^*} + 1 \right) - 1 \right)^{-2}. \quad (4)$$

Both A_ν and s_f are now proportional to the absolute value of the velocity, making the hydrodynamic model non-linear. The number of calibration parameters is again reduced to one: the dimensionless roughness height z_0^* .

As the velocity is expanded into a series $u^0 + u^1 + \dots$, the eddy viscosity and partial-slip parameter in (3)-(4) should also be expanded into similar series. We therefore obtain series $A_\nu^0 + A_\nu^1 + \dots$ and $s_f^0 + s_f^1 + \dots$. In the model, the leading-order eddy viscosity and partial slip parameter represent the roughness of the system and remain part of the differential equation. The higher-order eddy viscosity and partial slip terms appear as forcing terms. The velocity u^n at order n depends on A_ν^n and s_f^n , while A_ν^n and s_f^n in turn depend on u^n . This

non-linear interaction is sketched in Figure 4. At leading order, the model is fully non-linear as the tidal flow determines the leading-order eddy viscosity, which in turn affects the tidal flow. On the higher orders, all the physical mechanisms that act at this order determine the eddy viscosity at that order. However, since the eddy viscosity at higher orders appear as a forcing term, it only appears in one physical mechanism: the mixing term. Therefore all mechanisms, except for the mixing term, are independent of the eddy viscosity at that order and so they are independent of other flow mechanisms at the same order. The different mechanisms contributing to the flow can thus still be separated even though the equations with the turbulence model (3)-(4) are non-linear.

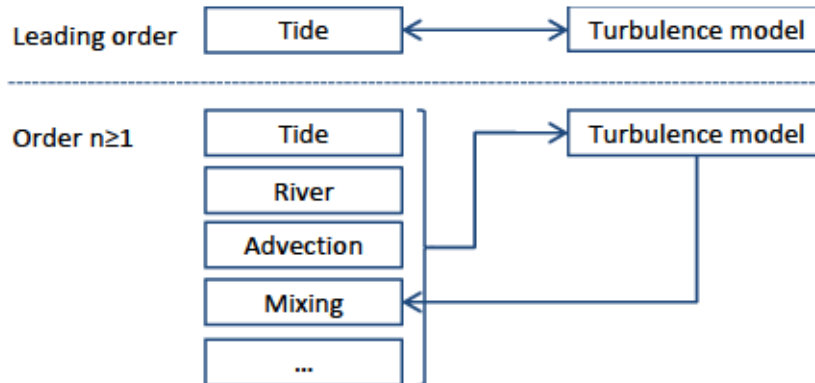


Figure 4 – Schematic overview of the physical mechanisms affecting the flow and their interaction with the turbulence model. At leading order, the tidal flow has a mutual interaction with the turbulence model. At higher orders, all mechanisms affect the higher-order turbulent mixing, but this in turn only affects a single turbulent mixing forcing component of the flow.

The eddy viscosity and partial-slip parameter in (3)-(4) vary in time due to the time-variation of $|u|$. Time-variations of the eddy viscosity are incorporated into the model of Brouwer *et al.* (2017) by using the method of Dijkstra (2014). Experiments will be done with and without time-variations of A_v and s_f so that the importance of such time-variations can be assessed.

The scaled approach relies on the higher-order eddy viscosity components being small compared to the leading-order eddy viscosity. This is not necessarily the case, especially near the landward end of the estuary, where the leading-order tide becomes relatively weak. We therefore include a user-defined minimum value for the leading-order sub-tidal eddy viscosity, which is relative to the depth but independent of the velocity, i.e.

$$A_v^0/H \geq (A_v/H)_{\min}.$$

2.3.3 Non-linear truncated formulation

The scaling of the eddy viscosity can still be compromised when including large time variations of the eddy viscosity. The scaled approach still converges, but the convergence is slow and results at different orders may oscillate so that one order approximately cancels another. This highly complicates the interpretation of the result. An alternative approach is to use a truncation of the result. In this approach all the different orders of magnitude of the eddy viscosity are added together and the hydrodynamic model only uses the total eddy viscosity. This approach is sketched in Figure 5. All physical mechanisms now affect the eddy viscosity, which in turn affects all physical flow mechanisms. The model is therefore fully non-linear and different contributions to the flow can therefore no longer strictly be separated.

The user-defined minimum eddy viscosity introduced above will also be used for the truncated formulation. Technically, this minimum is not required for the turbulence model, since the eddy viscosity is no longer ordered and depends on all flow components. However, the eddy viscosity varies on very short spatial scales near the landward end of the estuary, violating the scaling of the hydrodynamic model. A minimum eddy

viscosity can restrict the spatial variations to such extent that the scaling method for hydrodynamics is still satisfied.

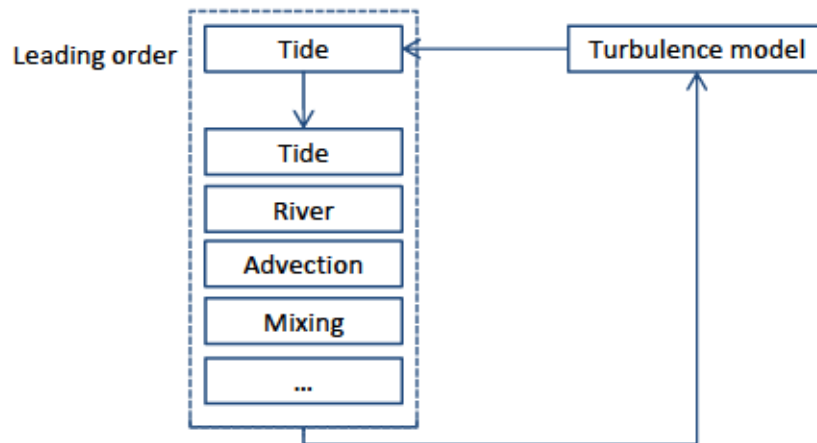


Figure 5 – Schematic overview of the truncated turbulence model approach. All physical flow mechanisms together form the input to the turbulence model. The turbulence model in turn affects all the physical flow mechanisms. The separate mechanisms can no longer be separated.

3 Results

3.1 Base model

3.1.1 Base model of Brouwer *et al.* (2017)

The base model for the Scheldt has been calibrated by Brouwer *et al.* (2017). They calibrated the model by using a cost function evaluating the RMS difference between model results and measurements. This has been done for a large range of the calibration parameters A_v and s_f . The result is presented in Figure 6a, which shows a large band of calibration parameters for which the cost function for the M_2 tide is very close to its minimum (blue colours). The exact minimum is denoted by the red dot. However, based on a visual judgement of the result, Brouwer *et al.* (2017) decided to use the values

$$\begin{aligned} A_v &= 0.061 \text{ m}^2/\text{s}, \\ s_f &= 0.003 \text{ m/s}, \end{aligned} \quad (5)$$

which is denoted by the yellow dot. Figure 6b shows the cost function for the M_4 tide. The minimum of this cost function (red dot) is on the edge of the domain at unrealistic values of the parameters. The base case is therefore not calibrated for the M_4 tide.

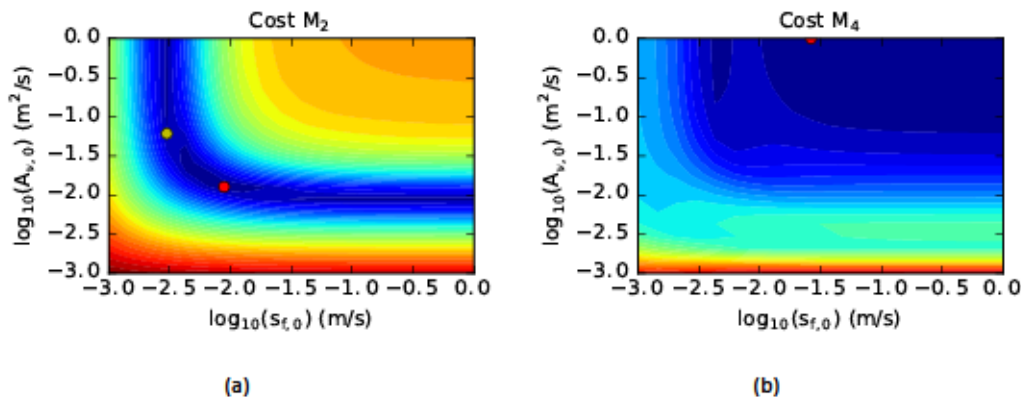


Figure 6 – Plot of the cost function that compares the fit between the measurements and model result for the M_2 tide (a) and M_4 tide (b). The cost function is computed for a range of the calibration parameters A_v and s_f . The blue colours indicate the smallest values of the cost function. The red dot denotes the minimum, while the yellow dot denotes the calibration chosen by Brouwer *et al.* (2017).

The water level amplitude and phase and the velocity amplitude for the calibrated base case with setting (5) are presented in Figure 7. There is a quite good correspondence between model result and measurements concerning the M_2 amplitude in the first half of the estuary, with a maximum error of about 10 cm. Also, there is good correspondence concerning the M_2 and M_4 phase, with maximum errors of 10 and 20 degrees respectively. The M_2 amplitude in the Upper Sea Scheldt and M_4 amplitude in the whole estuary are overestimated by up to 50 cm. In case of the M_4 tidal amplitude, this overestimation is more than 100% of the measured amplitude. The cross-sectionally averaged velocity is difficult to measure and maybe subject to large measurement errors. The comparison between measured and modelled velocity is therefore only indicative. That being said, the results for the M_2 and M_4 velocity (Figure 7c) show a similar pattern as seen for the surface elevation: the M_2 velocity is well approximated up to the Upper Sea Scheldt, while the M_4 velocity is overestimated in the whole estuary.

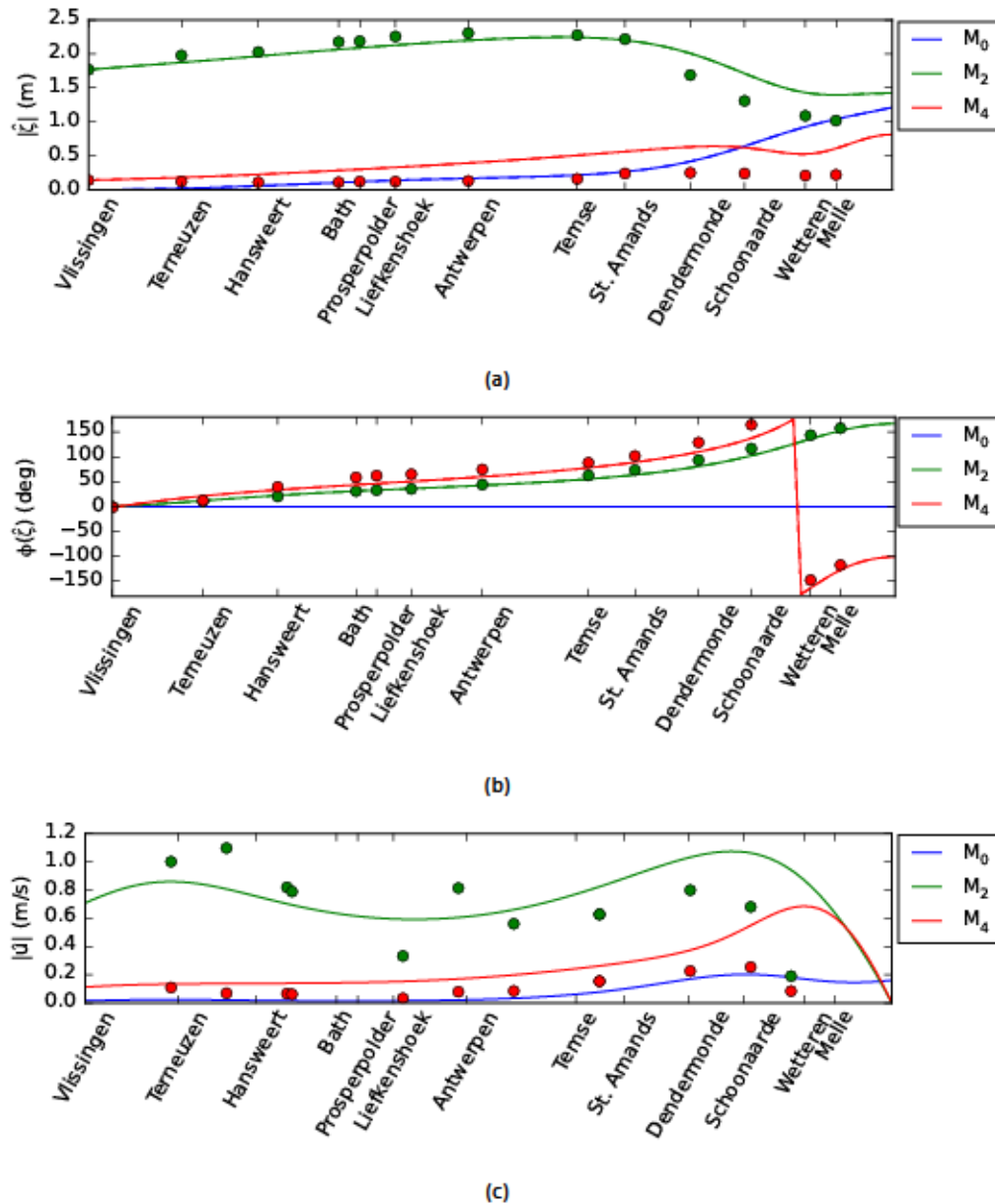


Figure 7 – Model results of the base model (solid lines) compared to measurements (dots) for the water level amplitude (a), water level phase (b) and depth-averaged velocity amplitude (c) along the Scheldt River. The place names on the horizontal axis correspond to the water level stations.

3.1.2 Linear single-parameter calibration

The two-parameter calibration presented in Figure 6 allows for a wide range of combinations of A_v and s_f . In this section we eliminate A_v as calibration parameter using relation 2 introduced in Section 2.3. This relation expresses A_v as a linear function of s_f and the local depth. The model is calibrated using the remaining parameter s_f , see Figure 8. The M_2 cost function now has a clear minimum for $s_f = 4.8 \cdot 10^{-3}$ m/s. The M_4 cost function on the other hand has a very flat minimum and is insensitive to large roughness values. We therefore prefer to calibrate the model solely on the M_2 tide.

Figure 9 shows the water level amplitude when using $s_f = 4.8 \cdot 10^{-3}$ m/s. Restricting our attention to the M_2 tide for the moment, we see that the water level amplitude is under-predicted by up to 15 cm in most of the estuary, while it is over-predicted in the Upper Sea Scheldt by up to 40 cm. There are only small differences compared to the base model. It can thus be concluded that the depth-dependence of the eddy viscosity that is

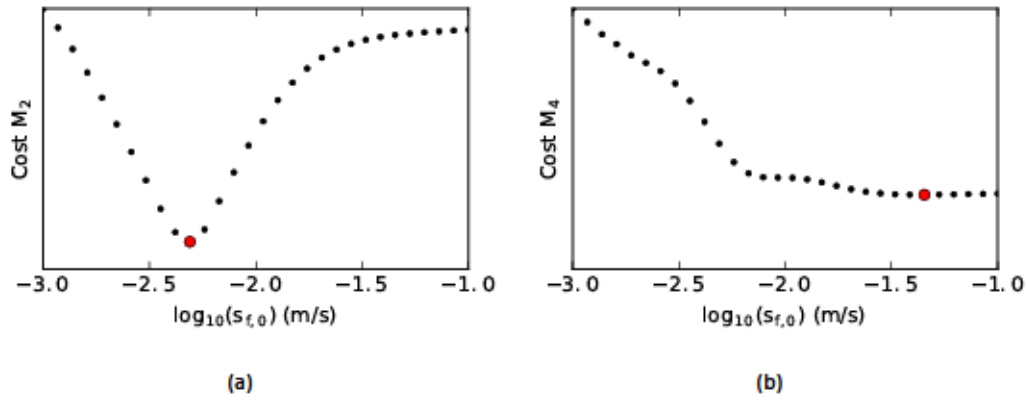


Figure 8 – Cost function for the M_2 tide (a) and M_4 tide (b) as a function of the calibration parameter s_f . The red dots indicate the minimum values attained.

now contained in the model neither improves nor worsens the result. This result is significant: it implies that it is possible to replace the two calibration parameters in the base model by a single calibration parameter with similarly satisfactory results. This single parameter now has a single best value for calibration for the M_2 tide, which makes the results more robust.

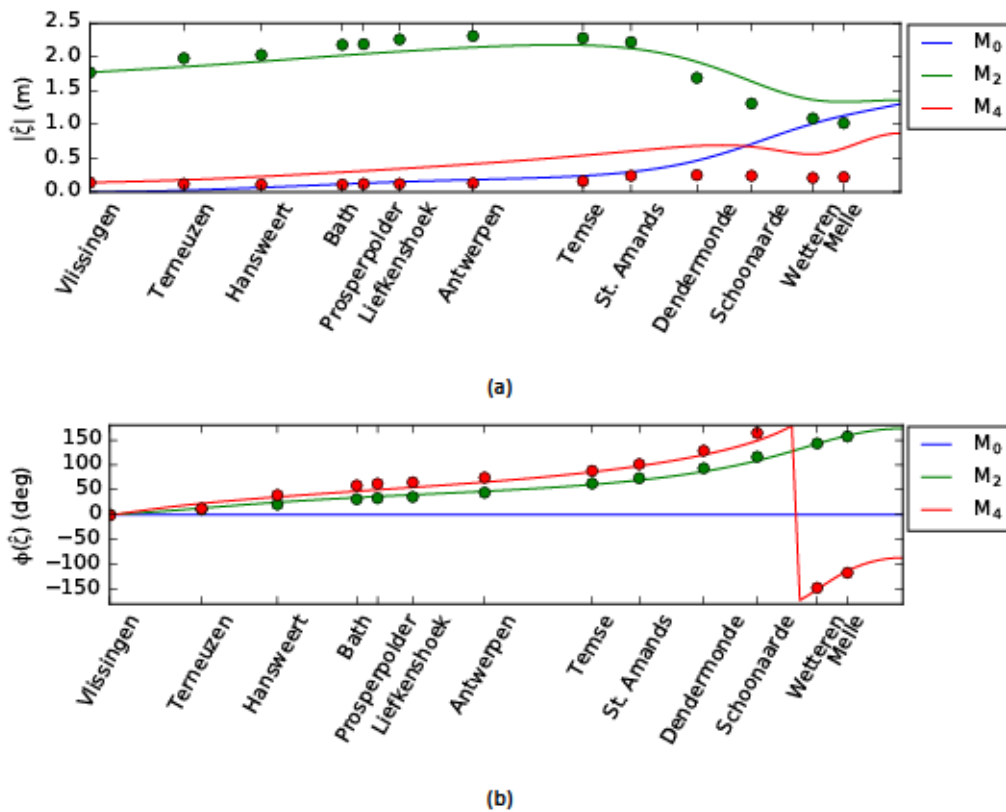


Figure 9 – Model results of the linear single-parameter model (solid lines) compared to measurements (dots) for the water level amplitude (a) and water level phase (b) along the Scheldt River. The place names on the horizontal axis correspond to the water level stations.

3.2 Higher-order dynamics

3.2.1 Higher-order water levels

The base model is extended by including higher-order dynamics. These dynamics include interactions between the tide and river as well as non-linear interactions of the tide and the dependency of the eddy viscosity on the sub-tidal water level set-up. It is chosen to keep the same value of the calibration parameter $s_f = 4.8 \cdot 10^{-3}$ m/s as before. This allows for a clear comparison between the base model and the model with higher-order dynamics. Here we include all the higher-order dynamics up to the sixth order.

The resulting water level amplitude is shown in Figure 10. The dashed lines shows the water level amplitude of the leading and first order and are the same as in Figure 9. The solid lines show the water level amplitude including the higher order dynamics. The higher order dynamics are only relevant in the Upper Sea Scheldt and most notable upstream of Dendermonde. It is clear from the figure that the higher-order dynamics does not lead to a better correspondence between the model and the measurements. Both the M_2 and M_4 tides are strongly amplified near the tidal weir. As a consequence, the tidal amplitude of both components is over-estimated by approximately one meter at the weir. The phases, which were approximated well in the base model, now start to deviate from the measurements upstream of Dendermonde.

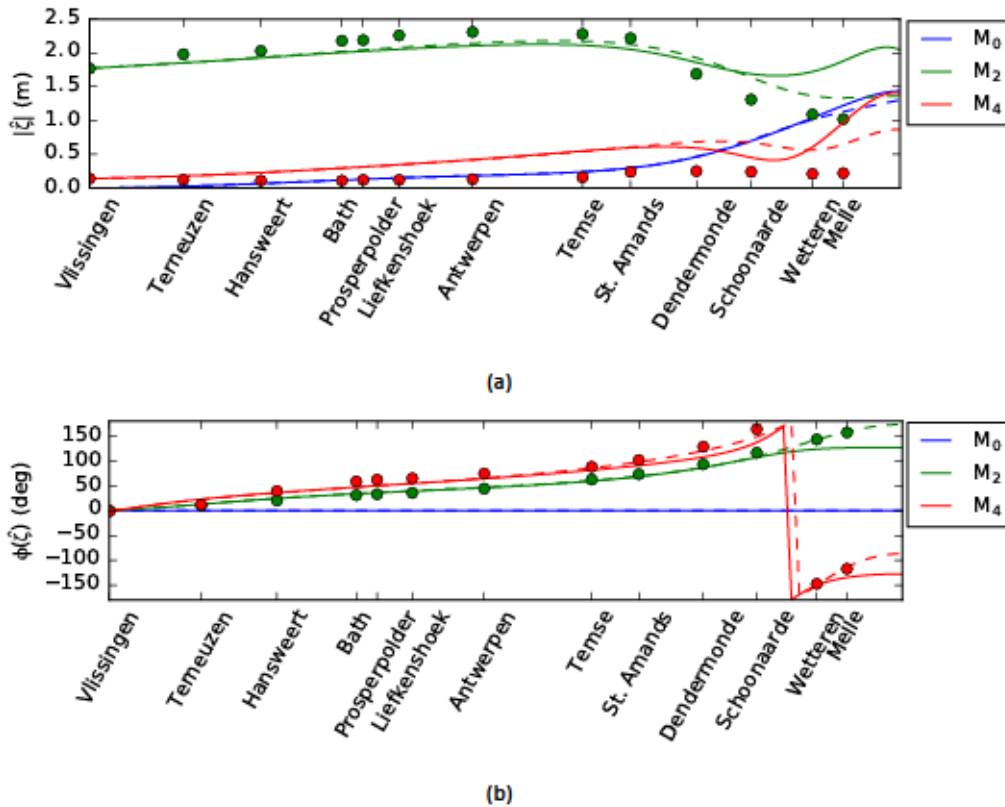


Figure 10 – Model results of the higher-order linear single-parameter model (solid lines) compared to the first-order model (dashed lines) and to measurements (dots) for the water level amplitude (a) and water level phase (b) along the Scheldt River. The place names on the horizontal axis correspond to the water level stations.

The contributions at the sixth order have a typical maximum water level amplitude of 20 cm close to the weir. A tenth-order computation has been done in order to verify that the orders beyond the sixth are not significant. This computation shows that the magnitude of the surface elevation and velocity is smaller at each subsequent order. Individual tenth-order components have a maximum amplitude of under 10 cm. Many of these components cancel each other, so that the maximum difference between computation up to sixth and tenth order is approximately 10 cm in the sub-tidal, M_2 and M_4 water level amplitudes. Since the orders up to

the sixth cover most of the higher-order dynamics and in order to limit computational time, it is chosen take the sixth order as the maximum for all further experiments.

3.2.2 Decomposition of the second-order dynamics

In order to explain the higher-order results, we will look closer at the second-order tidal elevation, see Figure 11. The second-order hydrodynamics consists of four mechanisms, which are all non-linear interactions between lower-order components of the water motion. The major contributions are the tidal return flow, no-stress and mixing components. The tidal return flow and no-stress components are both corrections to the tide due to flow between the reference level $z = 0$ and the actual surface level. The effect of both is to amplify the M_2 tide in the Upper Sea Scheldt. This can be understood intuitively by noting that the actual surface level, on average, is above the reference level in the Upper Sea Scheldt, seen from the subtidal water level set-up. Hence the actual depth is larger than the reference depth. The large reduction in depth in the Upper Sea Scheldt is the reason that the tidal wave amplitude damps strongly. Therefore, a correction to a larger depth leads to less damping of the tidal wave.

The mixing component represents the increased level of mixing when the actual surface level is above the reference level, see also Figure 12. The figure shows the eddy viscosity over the length of the estuary, with the leading-order eddy viscosity (dashed line) and the total eddy viscosity up to the sixth order (solid line). The eddy viscosity decreases with the along-channel distance. This is due to the decreasing depth, as is also illustrated in the right panel, which shows the eddy viscosity relative to the depth. The higher-order effects add turbulent mixing to the end of the estuary, due to the set-up of the water level by the river discharge and non-linear effects of the tide. At the tidal weir, this added mixing amounts to 50% of the leading-order eddy viscosity. It can thus not be neglected. The increased mixing leads to an increased damping of the tidal wave (Figure 11) in the Upper Sea Scheldt past Dendermonde. The mixing component thus counteracts the tidal amplification by the tidal return flow and no-stress component. However, the net effect of all higher-order components is still a pronounced amplification of the tide in the Upper Sea Scheldt.

Effects similar to those at second order can be observed in the fourth and sixth order. The third and fifth order only affect the subtidal and M_4 flow, which we will not discuss in this section.

3.2.3 Tide-river interaction

Most of the higher-order dynamics result from non-linear interactions between the external M_2 and M_4 tide. However tide-river interactions are also contained in the higher-order dynamics. Through these interactions, variations of the river discharge can affect the tidal amplitude. This is the reason to investigate the effect of changing the river discharge.

The tide-river interaction is present in all the higher-order components, such as were presented in Figure 11. Though the model can explicitly display all interactions between the tide and the river discharge separately, it is more intuitive to plot the total water level amplitude for several river discharges. Figure 13 plots the water level amplitude for cases with typical summer ($Q = 20 \text{ m}^3/\text{s}$) and winter ($Q = 70 \text{ m}^3/\text{s}$) discharges. The effects of the river discharge on the M_2 and M_4 tide are clearly very small. In this model, an increase in the river discharge leads to a small reduction of the M_2 and M_4 tidal amplitude near the weir.

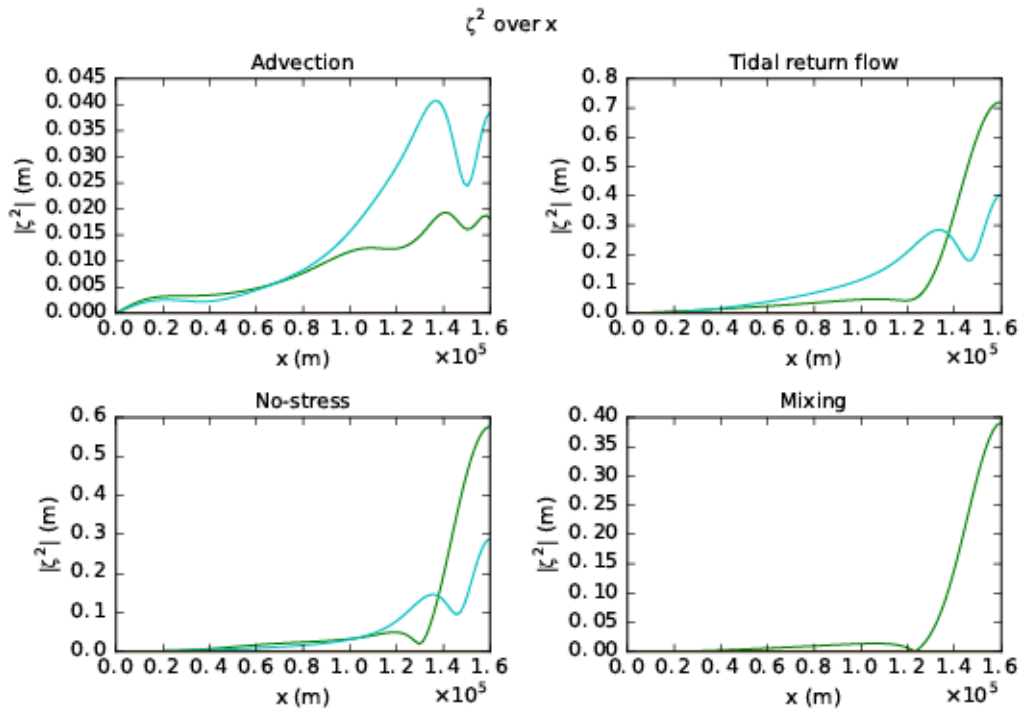


Figure 11 – Physical mechanism contributing to the second-order water level amplitude. The green lines indicate the M_2 contributions, while the cyan lines denote the M_6 contributions. The physical mechanism are explained in 2. The advection term is small and can be disregarded. The tidal return flow and no-stress components have a phase corresponding to an amplification of the M_2 tide. The mixing component has a phase corresponding to damping of the tide.

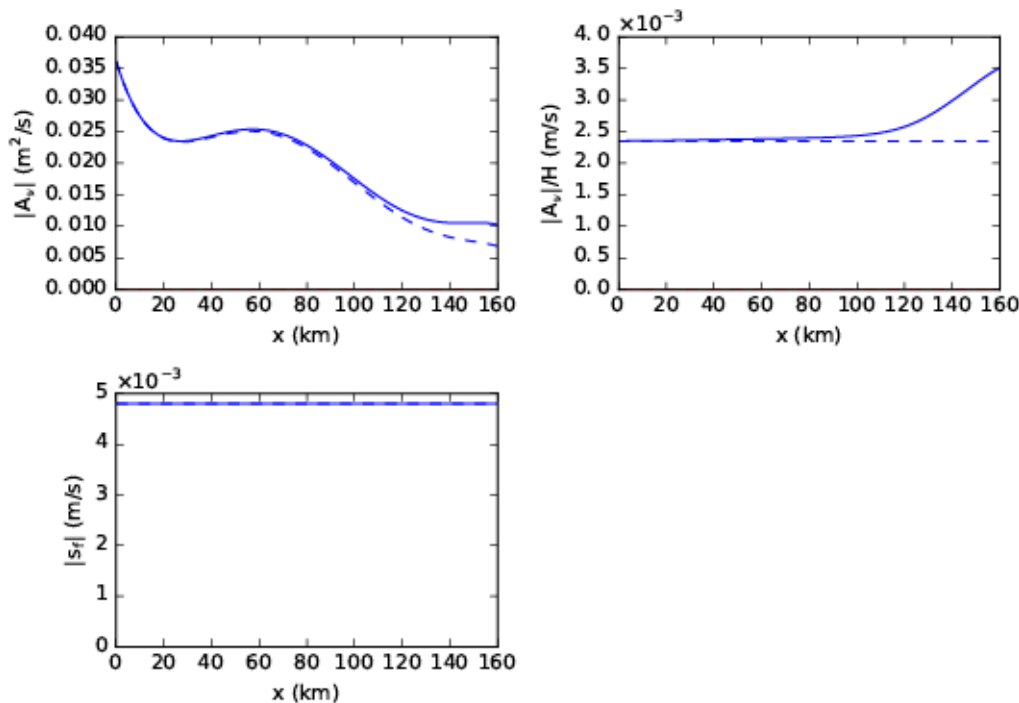


Figure 12 – Eddy viscosity, eddy viscosity scaled by the depth and roughness parameter s_f along the length of the estuary. Results are presented up to the first order (dashed lines) and sixth order (solid lines). The higher-order mixing terms add to the turbulent mixing at the landward end of the estuary, due to the sub-tidal water level set-up.

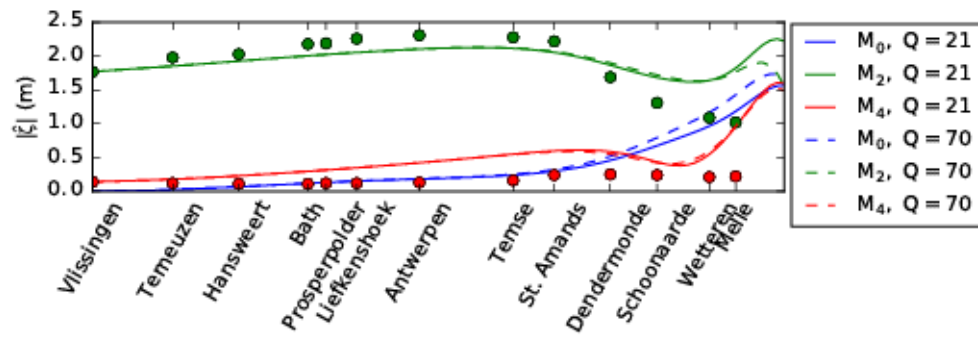


Figure 13 – Computed water level amplitude for typical summer ($Q = 20 \text{ m}^3/\text{s}$) and winter ($Q = 70 \text{ m}^3/\text{s}$) conditions up to the sixth order. The long-term year-average measurements are provided as reference (dots). The variation in river discharge only has a minimal effect on the tides.

3.3 Non-linear bottom friction

3.3.1 Constant eddy viscosity

The previous sections have taken the level of turbulent mixing as a constant or function of the local depth, but independent of the flow velocity. The bottom friction was taken as a linear function of the velocity. More realistically, the rate of turbulent mixing depends on the velocity magnitude and the bottom friction depends quadratically on the velocity. These dependencies lead to a non-linear model. Nevertheless, as was described in Section 2.3, it is still possible to analyse the different physical contributions from this non-linear model.

The dependence of the eddy viscosity and partial slip parameter on the velocity is incorporated by using turbulence closure (3)-(4). These equations take the dimensionless roughness height z_0^* as calibration parameter. Here we only use the sub-tidal component of the eddy viscosity and roughness coefficient; time-dependencies will be considered in the next section. The result of the calibration up to sixth order is presented in Figure 14. Again we find a clear minimum for the calibration of the M_2 tide, while we find a less pronounced minimum for the M_4 tide. We choose the best value for the M_2 tide, which equals $z_0^* = 0.0017$. The turbulence model additionally takes a minimum level of turbulent mixing at the leading order equal to $(A_\nu/H)_{\min} = 2 \cdot 10^{-3}$, $s_f = 4 \cdot 10^{-3}$, see also the description in Section 2.3. The background mixing is such that the leading-order mixing is always larger than the higher-order corrections. However, the background mixing is chosen small enough to have only minimal effects on the results.

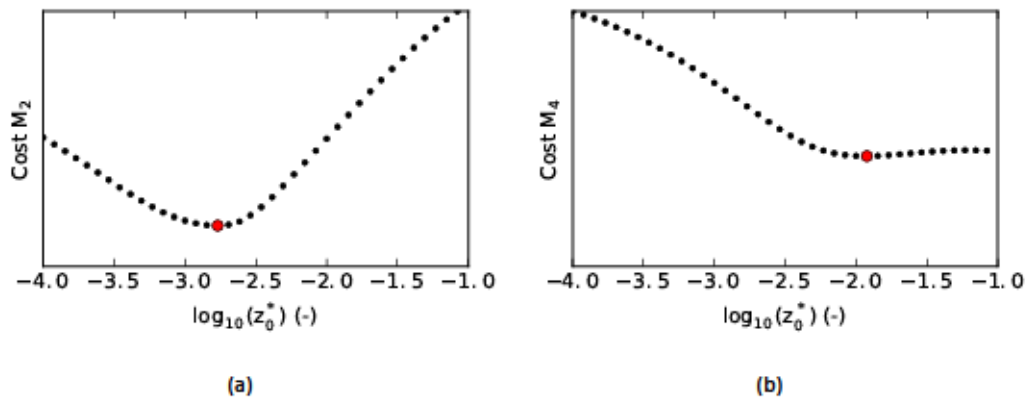


Figure 14 – Cost function for the M_2 tide (a) and M_4 tide (b) up to sixth order as a function of the calibration parameter $z_0^* = z_0/H$. The red dots indicate the minimum values attained.

The effect of the new turbulence model and bottom boundary condition is visualised in Figure 15. The figure shows A_ν , A_ν/H and s_f up to the first order (dashed lines) and up to the sixth order (solid line). There are a number of clear differences compared to the eddy viscosity in the linear model case (Figure 12), which are most clear from A_ν/H and s_f . These quantities have two local maxima. The first is in the Western Scheldt near Terneuzen. The second is in the Upper Sea Scheldt between Dendermonde and Wetteren. The maximum in the Upper Sea Scheldt is already clearly visible in the first-order simulation (dashed line), but becomes more pronounced in the higher-order computations (solid line). This peak in turbulent mixing and friction coincides with the reach where the measurements indicate a strong damping of the tidal wave.

The effects of this on the water level amplitude and phase and velocity amplitude are presented in Figure 16. The results up to the first order are again shown using dashed lines, while the results up to the sixth order are shown using solid lines. The figure shows a stronger damping of the tidal wave upstream of Dendermonde compared to the linear cases presented before. This is owed to the peak in the eddy viscosity and bottom friction. As a result, the first-order results no longer over-predict the M_2 water levels beyond Dendermonde. Also the M_4 tide is more damped, so that the computed M_4 water level amplitude is closer to the measurements. Nevertheless there is still a strong discrepancy between model result and measurements concerning the M_4

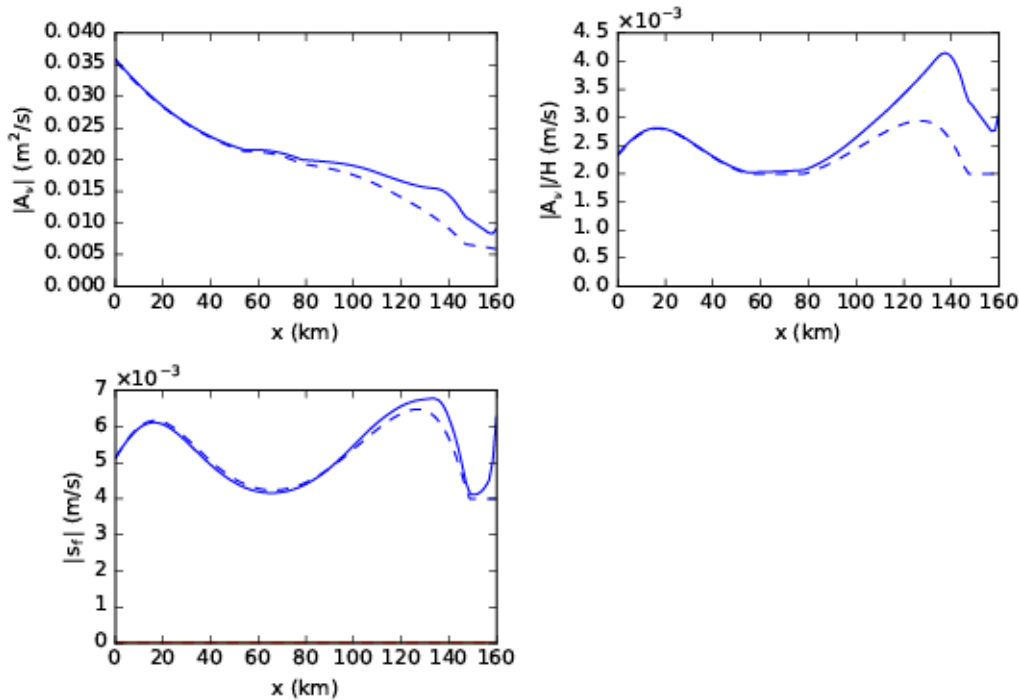


Figure 15 – Eddy viscosity, eddy viscosity scaled by the depth and partial slip parameter s_f along the length of the estuary. Results are presented up to the first order (dashed lines) and sixth order (solid lines). The eddy viscosity (relative to the depth) and roughness now have two distinct local maxima owing to the local peaks in the velocity. The maximum between 120 and 140 km coincides with the area of strong damping of the tide in the Upper Sea Scheldt.

tide. The higher-order effects lead to amplification of the tide. This amplification is smaller than with the linear model (previous section), but still leads to significant differences between model result and measurements. The effect of the higher-order dynamics on the water level phase show a significant improvement compared to the linear model. The phase computed by the first- and higher-order model are now similarly close to the measurements.

The higher-order computations seem to have a clear positive effect on the correspondence between the modelled and measured velocity magnitude. The M_2 velocities up to first order are similarly accurate as in the base model (compare Figure 7). However, the higher-order computations lead to a reduction of the M_2 velocity. This reduction corresponds to an overall reduction of the M_2 water level gradient due to higher-order effects beyond Dendermonde.

3.3.2 Time-dependent eddy viscosity

Up to now we have only considered the subtidal signal of the turbulent mixing. In reality, the level of turbulent mixing varies over the tidal cycle. For dominantly barotropic flows, the time-variations of turbulent mixing are induced by time-variations in the flow magnitude and water level. Here we will take the M_2 and M_4 variations of the eddy viscosity into account. Higher frequency eddy viscosity components are not considered in this section, although they are definitely present. An experiment that included the M_6 , M_8 and M_{10} mixing components showed that the effect off these components on the M_2 and M_4 eddy viscosity are relatively small.

In the previous sections, the eddy viscosity was ordered with respect to ϵ . This ordering is violated when taking the time-varying eddy viscosity into account. This is mainly due to the M_2 mixing component that appears at the first order. This component becomes of the same order of magnitude as the leading-order mixing in the

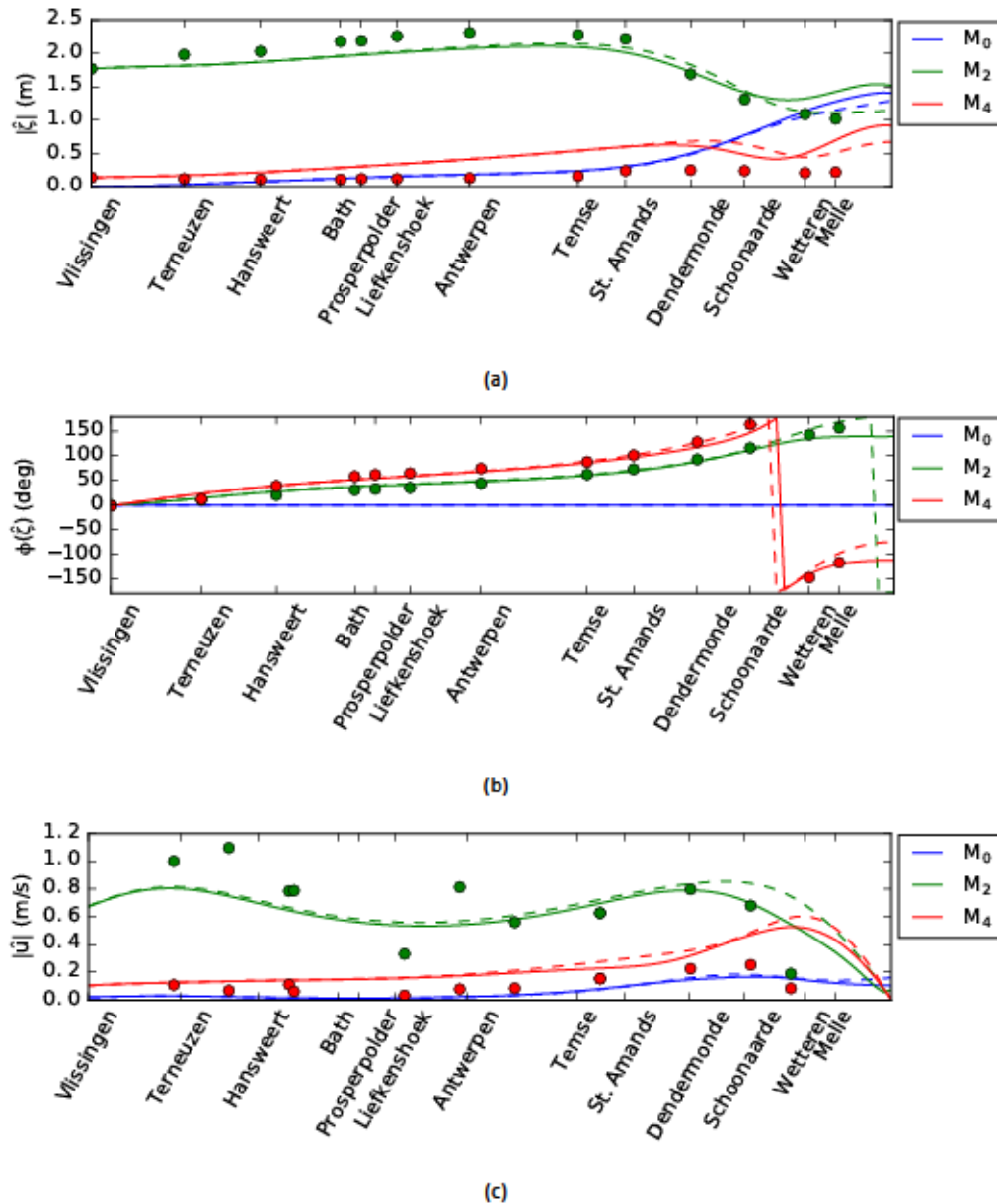


Figure 16 – Model results of the non-linear model at first order (dashed lines) and sixth order (solid lines) compared to measurements (dots) for the water level amplitude (a), water level phase (b) and depth-averaged velocity amplitude (c) along the Scheldt River. The place names on the horizontal axis correspond to the water level stations.

back of the estuary. The result is a highly oscillating and very slowly converging result in the higher-order computations. The robustness and interpretation of the higher-order results is therefore strongly challenged by this M_2 mixing component. As solution we include all first- and higher-order changes to the eddy viscosity at the leading order, as was described in Section 2.3.3

To illustrate the time-variations of turbulent mixing, we consider the the model up to the sixth order using a time-dependent eddy viscosity. The calibrated result, in this case, uses $\alpha_0^* = 0.001$. Figure 17 presents the resulting eddy viscosity, eddy viscosity relative to the depth and partial slip parameter s_f along the estuary. A dominant feature is the M_4 eddy viscosity component, which has an amplitude of roughly half the subtidal eddy viscosity amplitude in the Western Scheldt. The M_4 eddy viscosity implies that the level of turbulence is above average during the peak tides and less than average during the slack tides. The most dominant effect of the M_4 eddy viscosity is a damping of the M_2 tide. The added damping by the M_4 eddy viscosity is compensated for by a lower roughness and lower subtidal eddy viscosity than in the case without time-varying

mixing (compare Figure 12). This is so that the M_2 tide fits the measurements as well as possible.

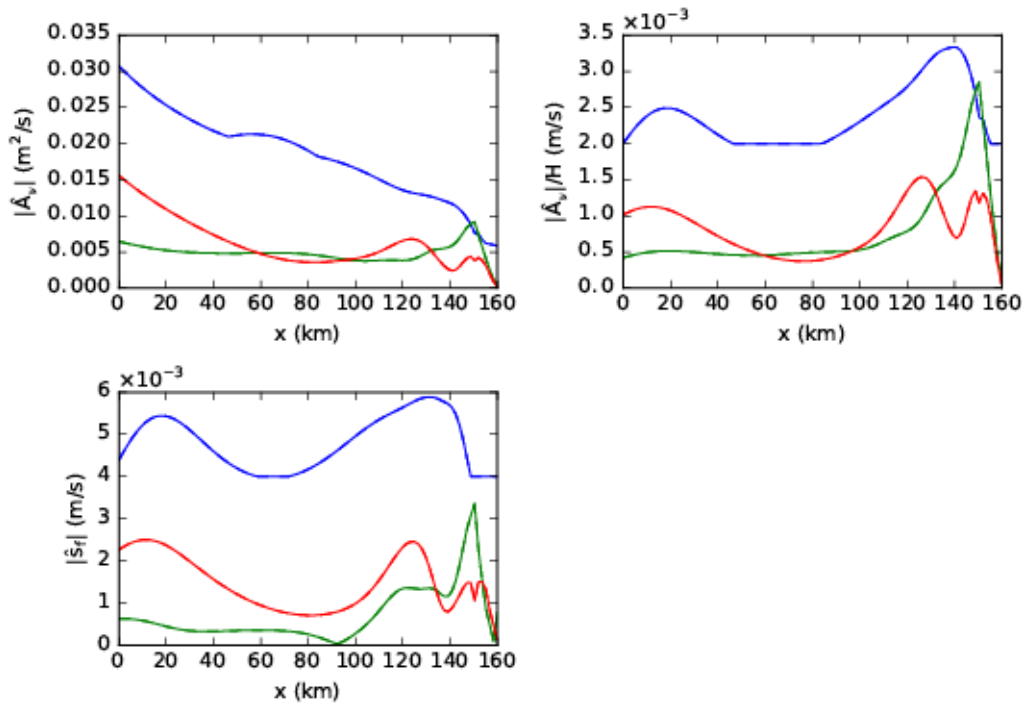


Figure 17 – Eddy viscosity, eddy viscosity scaled by the depth and roughness parameter s_f along the length of the estuary. The figure not only displays the sub-tidal component (blue), but also the M_2 (green) and M_4 (red) components. Results are for the non-linear model up to the sixth order. The M_4 component is mainly induced by the M_2 tide and is typically half the amplitude of the subtidal component in the Western Scheldt. The M_2 component is mainly induced by water level variations of the M_2 tide and by tidal asymmetry. It is mainly large near the landward end of the estuary.

The M_2 eddy viscosity is also important, especially in the Sea Scheldt. Part of this is due to the movement of the surface level. As the turbulent mixing scales with the depth, the M_2 tidal water level variation influences the turbulent mixing. Another important contribution is the interaction between the M_2 tide and the subtidal flow and M_4 tide. These interactions lead to tidal asymmetry, which implies that the peak ebb and peak flood tide are not of the same magnitude. As a result, also the turbulent mixing is unequal during peak ebb and peak flood, which is reflected in an M_2 variation of the eddy viscosity. The M_2 eddy viscosity does not have any effect on the M_2 tide up to first order. However, it does affect the subtidal flow and M_4 tide. The M_2 eddy viscosity adds a strong amplification of the sub-tidal water level in the first-order mixing component. However, this does not result into a higher total water level than in the previous section, because the subtidal water level of other components (no-stress, advection, tidal return flow) are smaller.

The water level amplitudes, phases and velocity amplitudes are shown in Figure 18. The M_2 tide up to first order (dashed green line) now damps more in the Upper Sea Scheldt than in any of the previous cases, so that the measurements are even under-predicted. This additional damping is mainly induced by the inclusion of the M_4 mixing component. However, the higher-order mechanisms (solid green line) again lead to amplification, so that the total M_2 water level over-predicts the measurements. The M_4 water levels are better predicted than in any of the previous cases (compare Figures 9, 10, 16). However the error in the M_4 component is still large, with maximum errors of more than 100% compared to the measurements. The measured and modelled M_2 and M_4 water level phases on the other hand correspond closely in the higher-order computations. The M_2 velocities are similarly accurate as in the previous cases, while the M_4 velocities are somewhat smaller and correspond more closely to the measurements. This is true for most of the estuary, except for the final 20 km of the estuary, where the modelled peak in M_4 currents cannot be observed in the measurements.

One can conclude that the time-dependency of the eddy viscosity adds a physical mechanism that yields a

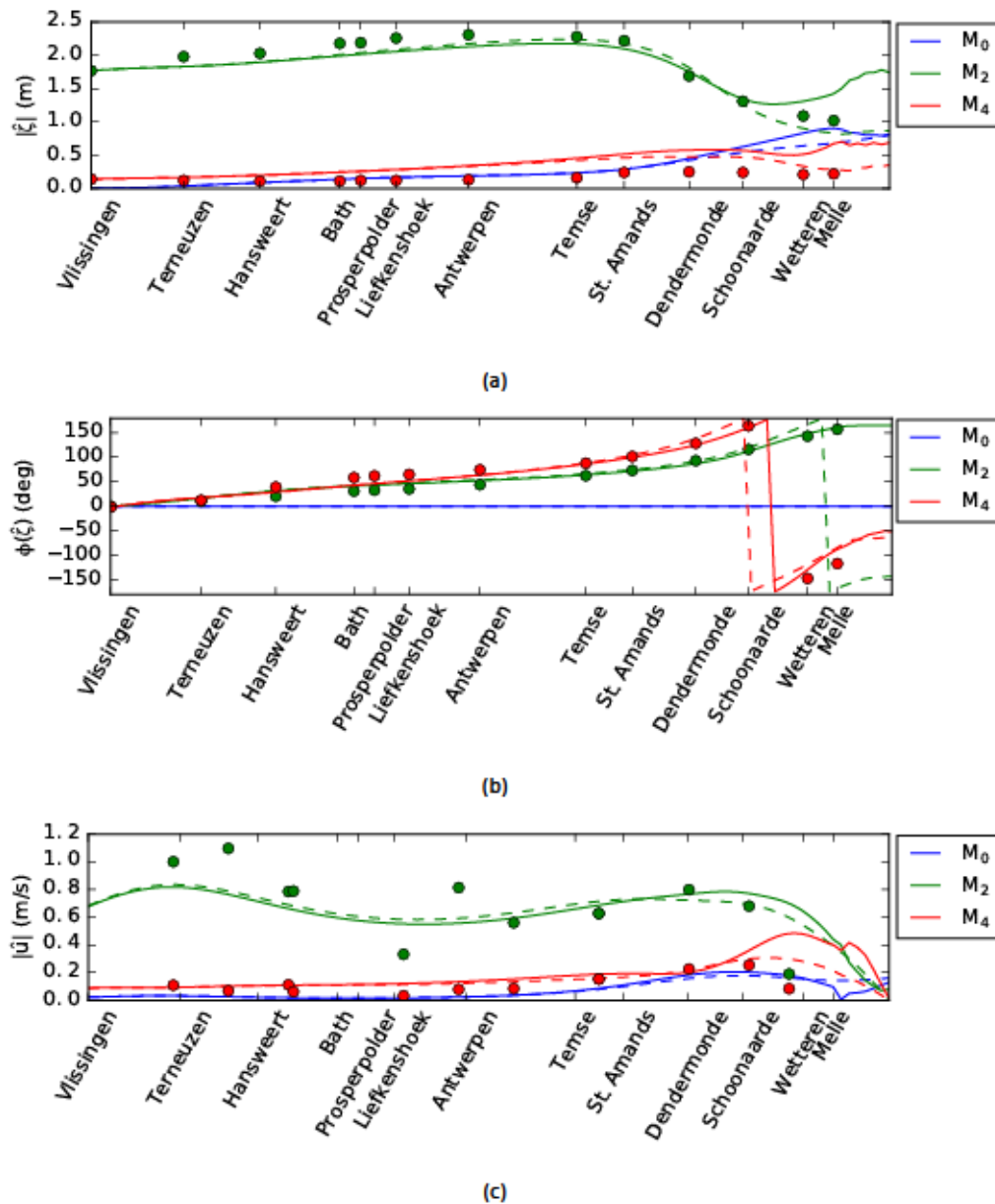


Figure 18 – Model results of the non-linear model with time-varying eddy viscosity at first order (dashed lines) and sixth order (solid lines) compared to measurements (dots) for the water level amplitude (a), water level phase (b) and depth-averaged velocity amplitude (c) along the Scheldt River. The place names on the horizontal axis correspond to the water level stations.

better prediction of the water levels and depth-averaged velocities. However, this improvement is mainly quantitative. The price for including the time-dependent eddy viscosity is the lack of a scaling of the eddy viscosity and additional computation time. It is therefore questionable whether the advantages of the time-dependent eddy viscosity compensate for the disadvantages for hydrodynamic computations. One of the more dominant effects of the time-dependent eddy viscosity has not yet been discussed here. The time-dependent eddy viscosity strongly increases the exchange flow compared to constant eddy viscosity models (Dijkstra *et al.*, 2017a). This can have a significant effect on the sediment transport. It is therefore still possible that the time-depend eddy viscosity has a significant effect on the sediment transport.

3.4 Consequences for tidal asymmetry

The previous sections have discussed several variations on the base model, and have assessed their effect on the surface elevation and velocity. Here we will look closer at the effect of the model variations on tidal asymmetry. Tidal asymmetry is an important indicator for the direction of the sediment transport. Here we will consider tidal asymmetry of the horizontal tide (velocities), as this is most indicative for the sediment transport. Measures for tidal asymmetry derived from the velocity are never fully conclusive about the direction of sediment transport, but they provide a reasonable indication. Therefore the terms *ebb dominant* and *flood dominant* to indicate the direction of tidal asymmetry are therefore defined here as the indicative direction of the net sediment transport. We will consider two measures for tidal asymmetry: slack water duration and the third power of the velocity.

The duration of slack water is especially important for the asymmetry in the sediment concentration. If high water slack (HWS; the slack tide between flood and ebb) is shorter than low water slack (LWS), sediment has relatively more time to settle before the flood tide. The concentrations are therefore relatively low at the beginning of flood. The concentrations increase during flood and only decrease a little during the short high water slack tide. The concentrations are therefore relatively large at the beginning of the ebb tide. Therefore, based on the concentrations, we can state that $T_{HWS} < T_{LWS}$ indicates ebb dominance, while $T_{HWS} > T_{LWS}$ indicates flood dominance. The high to low slack water ratio can be estimated using $\Delta\phi = \phi(u_{M_4}) - 2\phi(u_{M_2})$, where $\phi(u_{M_2})$, $\phi(u_{M_4})$ are the M_2 and M_4 velocity phases. It follows that

$$\Delta\phi \in \begin{cases} (0, \pi) & \text{then } T_{HWS} < T_{LWS} \text{ (ebb dominance)} \\ (\pi, 2\pi) & \text{then } T_{HWS} > T_{LWS} \text{ (flood dominance)} \end{cases}.$$

The mean of the third power of the velocity is an approximate measure for the bed-load sediment transport. Although less directly, the same measure also provides an indication for the transport of suspended sediments. A negative value of u^3 indicates ebb dominance, while a positive value indicates flood dominance. Both measures for asymmetry need to be considered to make a robust estimate of the suspended sediment transport direction.

The two measures for tidal asymmetry are plotted in Figure 19 for all model configurations tested in the previous sections. The base model computes up to the first order, while all other simulations compute up to the sixth order. The high to low slack water ratios (Figure 19a) are fairly consistent across the different model configurations. The HWS time is consistently shorter than the LWS time, indicating ebb dominance. The level of difference between T_{HWS} and T_{LWS} differs between the models in the Upper Sea Scheldt. The non-linear time dependent simulation consistently yields a lower T_{HWS}/T_{LWS} ratio and predicts a small reach of flood dominance in the Upper Sea Scheldt. The measurements display a large range of scatter, so that it is hard to say which of the model configurations is closer to the observations.

The values for the time-average of u^3 are also similar between the different model configurations in the Western and Lower Sea Scheldt. The asymmetry measure indicates ebb dominance at the mouth and flood dominance upstream of Hansweert. Note that the two measures for asymmetry do not agree in this domain. The real direction of sediment transport can therefore only be assessed by a full sediment model. The values of u^3 are more diverse between the different model configurations in the Upper Sea Scheldt. The non-linear time-dependent eddy viscosity model already predicts a zone of ebb dominance starting from Temse. The single-parameter model places this zone 10 km further upstream at St. Amands, while the base model again places it 10 km further upstream at Dendermonde. The non-linear model without time-dependent eddy viscosity predicts flood dominance throughout the estuary. All model configurations also predict a peak in the flood dominance beyond Dendermonde, but the exact location and magnitude of this peak varies. The comparison with measurements, which show a significant scatter and uncertainty, is inconclusive about which of the model configurations is the best.

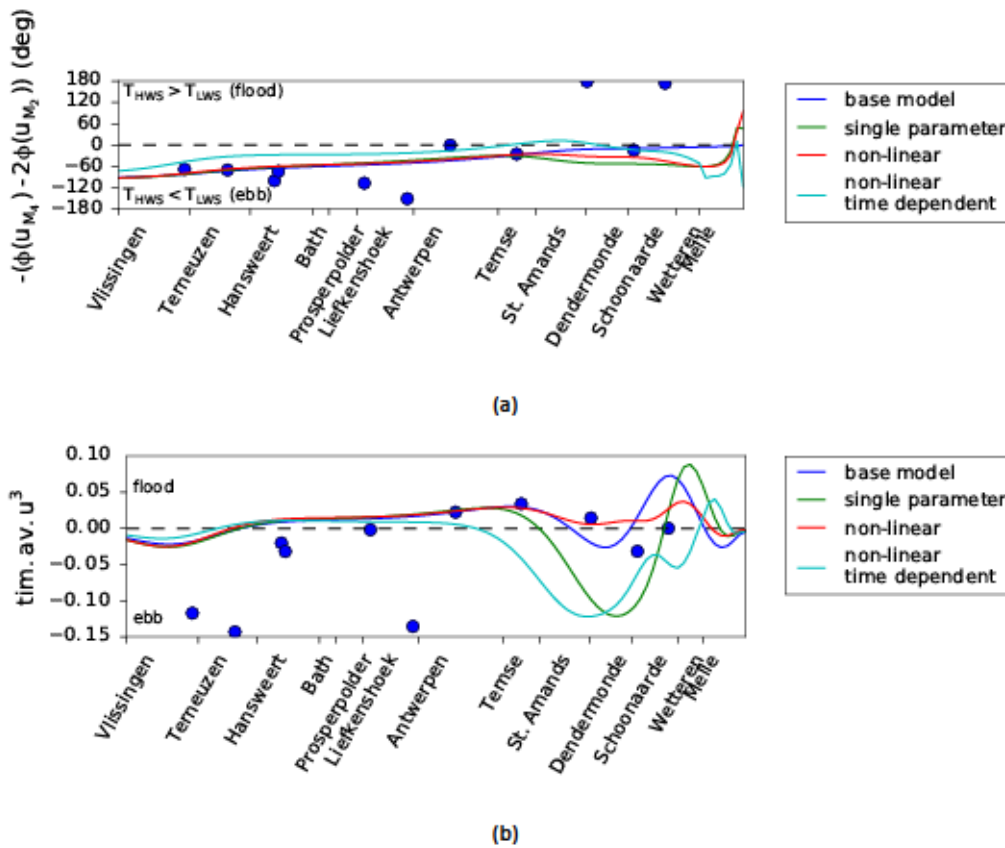


Figure 19 – Two measures for the tidal asymmetry for four different model configurations. The base model computes up to the first order, while the other configurations compute up to the sixth order. Figure a) shows the difference in time for high water slack and low water slack. $T_{HWS} < T_{LWS}$ indicates ebb dominance. Figure b) shows the time-averaged part of the velocity to the power three. Negative values indicate ebb dominance. The model configurations show fairly similar trends, while the measurements are highly scattered.

4 Conclusions

The objective for this study has been twofold. First objective has been to provide a more robust calibration procedure with a single best value of the calibration parameter or parameters. Second objective has been to improve the base model of Brouwer *et al.* (2017), so that the match between the computed and measured tidal elevation improves. To this end we have reconsidered the formulation of turbulence mixing and implemented higher-order non-linear hydrodynamics.

The idealised model manages to reproduce the measurement results fairly well. The qualitative behaviour of the M_2 and M_4 tide is captured. Quantitatively, the model predicts the M_2 tide well up to the Upper Sea Scheldt. The damping of the M_2 tidal wave in the Upper Sea Scheldt beyond Dendermonde can almost be fully captured using a non-linear formulation for the turbulence model and bottom friction. Although the modelled M_4 tidal water levels have the correct order of magnitude, they are over-predicted by up to more than 100%, even with a non-linear turbulence model. Several possible reasons have been identified. Firstly, three-dimensional effects might be important, especially for the level of turbulent mixing. Secondly, the length of the estuary might not be correctly described. The Scheldt River has two branches beyond Melle, which each have a different length and width. The exact length of the estuary and the effectiveness of the tidal reflection at the locks and weirs are therefore difficult to determine. Thirdly, it has been assumed here that the roughness of the system scales linearly with the depth. This is not necessarily true. Within our modelling framework we can conclude that the roughness does not scale linearly with the depth, but should, relatively, be larger in the Upper Sea Scheldt. However, an added along-channel dependency of the roughness adds a degree of arbitrariness to the model. It is therefore advised to keep the roughness formulation unchanged, unless there is clear observational evidence that justifies any along-channel variation of the roughness (e.g. a different bed composition). Finally, an alternative to changing to roughness in the Upper Sea Scheldt is to change the representative depth. The depth used in the current model is the width-averaged depth compared to the local mean water level. It remains unclear whether the width-averaged or the thalweg depth are the most representative values for use in a 2DV model. It is however advised in the future to use any of these depths compared to mean-sea level instead of local mean water level.

Summarising, we have found the following results:

1. Fitting the uniform eddy viscosity profile to results of the $k - \epsilon$ model, we find a simple linear relation between the calibration parameters s_f and A_v . This effectively reduces the number of calibration parameters to one. The quality of the calibration with one or two parameters is similar.
2. The higher-order dynamics (i.e. $>$ first order) are insignificant in the Western Scheldt and Lower Sea Scheldt.
3. The higher-order dynamics have a strong effect on the water level amplitude and velocity in the Upper Sea Scheldt, especially beyond Dendermonde. The result is an amplification of the M_2 and M_4 water level. The effect on the velocity depends on the exact formulation of the eddy viscosity.
4. The most dominant terms in the higher-order dynamics are those due to the surface linearisation: the no-stress correction and tidal return flow. These contributions lead to the amplification of the tides in the Upper Sea Scheldt.
5. The water level set-up in the Upper Sea Scheldt causes additional turbulent mixing, which reduces the tidal amplification from the surface linearisation terms.
6. The effects of momentum advection are unimportant throughout the Scheldt estuary
7. Quadratic bottom friction and the velocity-dependent eddy viscosity are essential for reproducing the damping of the M_2 tide in the Upper Sea Scheldt. The peak in the tidal velocities in the Upper Sea

Scheldt lead to a high level of turbulent mixing, and therefore damping of the tide.

8. Including the M_2 and M_4 variations of turbulent mixing also add significantly to the damping of the tidal wave beyond Dendermonde.
9. The higher-order dynamics nor the eddy viscosity formulation lead to qualitative changes in the measures for tidal asymmetry.
10. The two studied measures for tidal asymmetry provide different conclusions as to the direction of the net sediment transport. A full sediment transport model is therefore required to be conclusive about the net sediment transport.

Concluding, The idealised model now has a robust linear and non-linear turbulence model that depends only on one calibration parameter. The non-linear formulations for the turbulence model and bottom boundary condition are advised for use in future projects, as they describe an important qualitative model dependency and quantitatively significantly improve the results in the Upper Sea Scheldt. The higher-order dynamics have a significant quantitative effect on the Upper Sea Scheldt, but do not clearly add to the understanding of the physical mechanisms at work in the Scheldt River estuary. The effect of the turbulence model formulation and higher-order dynamics on sediment transport is yet to be investigated and can only be determined by using a full sediment transport model.

References

- Brouwer, R. L.; Schramkowski, G. P.; Verwaest, T.; Mostaert, F. (2017). Geïdealiseerde processtudie van systeemovergangen naar hypertroebelheid. WP 1.3 Basismodel getij en zout. Versie 2.0. *WL Rapporten*, 13_103_3. Waterbouwkundig Laboratorium: Antwerpen, België
- Burchard, H.; Hetland, R. D.; Schulz, E.; Schuttelaars, H. M. (2011). Drivers of residual estuarine circulation in tidally energetic estuaries: Straight and irrotational channels with parabolic cross section. *Journal of Physical Oceanography* 41: 548–570
- Chernetsky, A. S.; Schuttelaars, H. M.; Talke, S. A. (2010). The effect of tidal asymmetry and temporal settling lag on sediment trapping in tidal estuaries. *Ocean Dynamics* 60: 1219–1241
- Dijkstra, Y. M. (2016). *Numerical 2DV coupled frequency perturbation model. Package for iFlow.*
- Dijkstra, Y. M. (2014). On the effect of tidal variations of turbulent mixing on flow and salt transport in estuaries. (mathesis). TU Delft
- Dijkstra, Y. M.; Schuttelaars, H. M.; Burchard, H. (2017a). Generation of exchange flows in estuaries by tidal and gravitational eddy viscosity - shear covariance (ESCO). *Journal of Geophysical Research: Oceans* 122: 4217–4237
- Dijkstra, Y. M.; Uittenbogaard, R. E.; Van Kester, J. A. T. M.; Pietrzak, J. D. (2016). In search of improving the numerical accuracy of the $k - \epsilon$ (open) model by a transformation to the $k - \tau$ model. *Ocean Modelling* 104: 129–142
- Dijkstra, Y. M.; Brouwer, R. L.; Schuttelaars, H. M.; Schramkowski, G. P. (2017b). The iFlow Modelling Framework v2.4. A modular idealised process-based model for flow and transport in estuaries. *Geoscientific Model Development* 10: 2691–2713. DOI: 10.5194/gmd-10-2691-2017
- Ianniello, J. P. (1977). Tidally induced residual currents in estuaries of constant breadth and depth. *Journal of Marine Research* 35: 755–786
- Ianniello, J. P. (1979). Tidally induced residual currents in estuaries of variable breadth and depth. *Journal of Physical Oceanography* 9: 962–974

A1 About the iFlow modelling framework

The iFlow modelling framework (Dijkstra *et al.*, 2017b) is a mathematical simulation tool that is especially developed for unravelling physical processes driving the flow and transport in estuaries and tidal rivers. A key feature of iFlow is its modular structure. This means that a 'base model', which only includes the most elementary physical mechanisms, can be easily extended by modules that implement more physical components. The complexity of the model can therefore easily be adjusted depending on the application at hand. Examples of modules in iFlow are the generator for domain geometry, turbulence model, several physical components for calculating hydrodynamics, the salinity model and sediment model. The modular structure enables users to cooperate by using existing modules written by others, together with their own modules, to create elaborate models adapted for specific situations.

iFlow also enables combinations of analytical and numerical modelling techniques. Analytical modelling is fast and accurate, but not always possible. Numerical modelling on the other hand is versatile, but comes with inaccuracies such as numerical diffusion, oscillations and limited accuracy of derivatives. By combining both techniques the model is as accurate and fast as possible, without restricting the range of applications.

The model finally contains automated modules for performing sensitivity analyses, calibration and plotting. These tools are generalised to perform analyses over any number of model parameters. This enables users to make a quick assessment and visualisation of the best model calibration and the sensitivity of the model to varying parameter values.

iFlow is free software under the GNU LGPL v3.0 license (see <https://www.gnu.org/licenses/lgpl-3.0.en.html>). The code and all manuals can be downloaded from [github.com](https://github.com/YoeriDijkstra/iFlow) under <https://github.com/YoeriDijkstra/iFlow>. This also includes a folder with various examples. Users who apply iFlow in any scientific publication, technical report or otherwise formal writing, are requested to cite Dijkstra *et al.* (2017b) but this is not compulsory.

A2 Model equations

A2.1 Hydrodynamics

A2.1.1 Leading-order and first-order model

The model scaling and derivation of the equations is discussed elaborately by Brouwer *et al.* (2017). Here we will mainly focus on the final set of equations and the differences of our model compared to Brouwer *et al.* (2017). As one of the main differences, our model allows for all tidal frequencies at all orders, while Brouwer *et al.* (2017) restrict their attention to the leading-order M_2 tide and first-order subtidal and M_4 tide. However, other frequencies may appear at both orders if the eddy viscosity and partial-slip parameter are allowed to vary in time. For the full derivation of this model we refer the reader to Dijkstra (2016).

We write the velocity and water level at order n as

$$\begin{aligned} u^n &= \Re \left(\sum_{f=-f_{\max}}^{f_{\max}} \hat{u}_f^n e^{fi\omega t} \right), \\ \zeta^n &= \Re \left(\sum_{f=-f_{\max}}^{f_{\max}} \hat{\zeta}_f^n e^{fi\omega t} \right), \end{aligned} \quad (\text{A-1})$$

where \hat{u}_f , $\hat{\zeta}_f$ are the complex amplitudes at the M_{2f} tidal frequency, ω is the angular frequency of the M_2 tide and f_{\max} is the maximum frequency component that is taken into account (here the M_{10} tide). The above expressions differ from Equation (1) presented in the main text by including also negative components ($f = -f_{\max}, \dots, -1$). This difference is however a matter of style, since

$$u^n = \Re \left(\sum_{f=-f_{\max}}^{f_{\max}} \hat{u}_f^n e^{fi\omega t} \right) = \Re \left(\sum_{f=0}^{f_{\max}} (\hat{u}_f^n + \overline{\hat{u}_{-f}^n}) e^{fi\omega t} \right).$$

Naturally, the same holds for ζ^n . Here we use Expression (A-1), because it is easier to write down the resulting set of matrix equations later if negative components are included. The equations are expressed in terms of the complex amplitudes which are written in vector form

$$\underline{\hat{u}}^n = [\hat{u}_{-f_{\max}}^n, \dots, \hat{u}_{-1}^n, \hat{u}_0^n, \hat{u}_1^n, \dots, \hat{u}_{f_{\max}}^n]^T \quad (\text{A-2})$$

$$\underline{\hat{\zeta}}^n = [\hat{\zeta}_{-f_{\max}}^n, \dots, \hat{\zeta}_{-1}^n, \hat{\zeta}_0^n, \hat{\zeta}_1^n, \dots, \hat{\zeta}_{f_{\max}}^n]^T. \quad (\text{A-3})$$

The leading-order dynamics is governed by the linear propagation of the tide, which includes the effects of bottom friction, convergence of the cross-section and reflection at the tidal weir. This dynamics is partly described by the momentum equation, which, using the vectors (A-2)-(A-3), reads

$$\begin{aligned} D\underline{\hat{u}}^0 - \left(N^0 \underline{\hat{u}}_z^0 \right)_z &= -g \underline{\hat{\zeta}}_x^0, \\ \bullet \quad N^0 \underline{\hat{u}}_z^0 &= 0 && \text{at } z = 0, \\ \bullet \quad N^0 \underline{\hat{u}}_z^0 &= S_f^0 \underline{\hat{u}}^0 && \text{at } z = -H, \end{aligned}$$

where D , \mathcal{N} and \mathcal{S}_f are matrices

$$D = \begin{bmatrix} -f_{\max}i\omega & & & \emptyset \\ & -(f_{\max} - 1)i\omega & & \\ & & \ddots & \\ \emptyset & & & f_{\max}i\omega \end{bmatrix},$$

$$\mathcal{N} = \frac{1}{2} \begin{bmatrix} 2\Re(\hat{A}_{\nu,0}) & \overline{\hat{A}_{\nu,1}} & \dots & \overline{\hat{A}_{\nu,f_{\max}}} \\ \hat{A}_{\nu,1} & 2\Re(\hat{A}_{\nu,0}) & \ddots & \vdots & \ddots & \emptyset \\ \vdots & \ddots & \ddots & \overline{\hat{A}_{\nu,1}} & \ddots & \\ \hat{A}_{\nu,f_{\max}} & \dots & \hat{A}_{\nu,1} & 2\Re(\hat{A}_{\nu,0}) & \overline{\hat{A}_{\nu,1}} & \dots & \overline{\hat{A}_{\nu,f_{\max}}} \\ & \ddots & & \hat{A}_{\nu,1} & \ddots & \ddots & \vdots \\ & \emptyset & \ddots & \vdots & \ddots & 2\Re(\hat{A}_{\nu,0}) & \overline{\hat{A}_{\nu,1}} \\ & & & \hat{A}_{\nu,f_{\max}} & \dots & \hat{A}_{\nu,1} & 2\Re(\hat{A}_{\nu,0}) \end{bmatrix},$$

$$\mathcal{S}_f = \frac{1}{2} \begin{bmatrix} 2\Re(\hat{s}_{f,0}) & \overline{\hat{s}_{f,1}} & \dots & \overline{\hat{s}_{f,f_{\max}}} \\ \hat{s}_{f,1} & 2\Re(\hat{s}_{f,0}) & \ddots & \vdots & \ddots & \emptyset \\ \vdots & \ddots & \ddots & \overline{\hat{s}_{f,1}} & \ddots & \\ \hat{s}_{f,f_{\max}} & \dots & \hat{s}_{f,1} & 2\Re(\hat{s}_{f,0}) & \overline{\hat{s}_{f,1}} & \dots & \overline{\hat{s}_{f,f_{\max}}} \\ & \ddots & & \hat{s}_{f,1} & \ddots & \ddots & \vdots \\ & \emptyset & \ddots & \vdots & \ddots & 2\Re(\hat{s}_{f,0}) & \overline{\hat{s}_{f,1}} \\ & & & \hat{s}_{f,f_{\max}} & \dots & \hat{s}_{f,1} & 2\Re(\hat{s}_{f,0}) \end{bmatrix}.$$

The remainder of the leading-order dynamics is described by the depth-integrated continuity equation

$$D\underline{\zeta}^0 + \frac{1}{B} \left(\int_{-H}^0 B\underline{u}^0 dz \right)_x = \underline{0} \quad (\text{A-4})$$

- $\underline{\zeta}^0(0) = \underline{A}^0$,
- $B(L) \int_{-H}^0 u^0(L, z) dz = 0$,

where \underline{A}^0 is the tidal amplitude at the mouth.

The first-order dynamics describes the linear propagation of the external M_4 tide and river flow, as well as the response to the baroclinic pressure induced by longitudinal salinity gradients and a first estimate of the non-linear interactions of the M_2 tide. The non-linear interactions of the M_2 tide typically results in a forcing at the subtidal and M_4 tidal frequency, although, again, other frequencies can be generated by time variations of the eddy viscosity and partial-slip parameter. The first-order momentum and depth-averaged continuity equations read

$$D\underline{\hat{u}}^1 - \left(\mathcal{N}^0 \underline{\hat{u}}^1 \right)_z = -g \underbrace{\underline{\zeta}_x^1}_{\text{advection}} - \underbrace{g\beta z \underline{\hat{s}}_x^0}_{\text{baroclinic}} + \underbrace{\underline{\xi}_z^1}_{\text{mixing}}, \quad (\text{A-5})$$

- $N\underline{\hat{u}}^1_z(x, 0) = \underbrace{-N\underline{\chi}^1}_{\text{no-stress}} - \underbrace{\underline{\xi}^1}_{\text{mixing}}$,
- $N\underline{\hat{u}}^1_z(x, -H) - \mathcal{S}_f^0 \underline{\hat{u}}^1(x, -H) = \underbrace{-\underline{\xi}^1 + \underline{\zeta}^1}_{\text{mixing}}$,

$$D\underline{\zeta}^1 + \frac{1}{B} \left(\int_{-H}^0 B\underline{u}^1 dz \right)_x = \underbrace{-\frac{1}{B} (B\underline{\gamma}^1)_x}_{\text{tidal return flow}} \quad (\text{A-6})$$

- $\underline{\zeta}^1(0) = \underbrace{\underline{A}^1}_{\text{tide}}$,
- $B(L) \int_{-H}^0 u^1(L, z) dz = \underbrace{-\underline{Q}^1}_{\text{river}} - \underbrace{B(L)\underline{\gamma}^1(L, t)}_{\text{tidal return flow}}$,

where

$$\begin{aligned} \eta^1(x, z, t) &= u^0 u_x^0 + w^0 u_z^0, && \text{(advection)} \\ \xi^1(x, z, t) &= A_\nu u_z, && \text{(mixing)} \\ \varsigma^1(x, t) &= s_f^1 u^0(x, -H, t), && \text{(mixing-roughness dependency)} \\ \chi^1(x, t) &= (A_\nu u_z(x, 0, t))_z \zeta^0, && \text{(no-stress)} \\ \gamma^1(x, t) &= u^0(x, 0, t) \zeta^0, && \text{(tidal return flow)} \end{aligned}$$

The seven forcing mechanisms of the first-order equations are indicated by the subscripts. The flow generated by each of these components can be analysed separately, because the equations are linear.

The vertical velocity w at both orders can be computed using the continuity equation, which is omitted here. Details of the continuity equation, derivation of the above vector equations and the numerical implementation can be found in Dijkstra (2016).

A2.1.2 Higher-order model

The higher-order equations do not contain any external forcing from the tide or river. Instead, they describe non-linear propagation of the tide, interaction between several tidal components and tide-river interaction. The derivation of the higher-order model is fully described by Dijkstra (2016). Here we present the equations.

In the following we use the notation

- $[\cdot]^n$ for n^{th} powers,
- $[\cdot]^{(n)}$ for n^{th} -order derivatives with respect to z ,
- $[\cdot]^{<n>}$ for n^{th} order in ϵ .

The momentum and depth-averaged continuity equations of order $n = 2, 3, \dots$ read

$$D\hat{u}^{<n>} - \left(N^{<0>} \hat{u}_z^{<n>} \right)_z = -g \hat{\zeta}_x^{<n>} \underbrace{- \hat{\eta}^{<n>}}_{\text{advection}} - \underbrace{\frac{g}{\rho_0} \int_z^0 \rho_x^{<n>}}_{\text{baroclinic}} - \underbrace{\hat{\beta}_\delta^{<n>}}_{\text{density-induced return flow}} + \underbrace{\hat{\xi}_z^{<n>}}_{\text{mixing}},$$

- $N^{<0>}(x, 0, t) \hat{u}_z^{<n>}(x, 0, t) = \underbrace{-\hat{\chi}^{<n>}}_{\text{no-stress}} - \underbrace{\hat{\xi}^{<n>}(x, 0, t) - \hat{\xi}_x^{<n>}}_{\text{mixing}},$
- $N^{<0>}(x, -H, t) \hat{u}_z^{<n>}(x, -H, t) - s_f^{<0>} \hat{u}^{<n>}(x, -H, t) = \underbrace{-\hat{\xi}^{<n>}(x, -H, t) + \hat{\zeta}^1}_{\text{mixing}},$

$$\hat{\zeta} + \frac{1}{B} \left(B \int_{-H}^0 \hat{u}^{<n>} dz \right)_x = \underbrace{-\frac{1}{B} (B \hat{\gamma}^{<n>})_x}_{\text{tidal return flow}},$$

- $\hat{\zeta}^{<n>}(0) = 0,$
- $B(L) \int_{-H}^0 \hat{u}^{<n>}(L) dz = \underbrace{-B(L) \hat{\gamma}^{<n>}(L, t)}_{\text{tidal return flow}},$

where

$$\eta^{<n>} = \sum_{m=0}^{n-1} u^{<m>} u_x^{<n-m-1>} + w^{<m>} u_z^{<n-m-1>}, \quad (\text{advection})$$

$$\beta_\rho^{<n>} = \frac{g}{\rho_0} \int_z^0 \rho_x^{<n>}, \quad (\text{baroclinic pressure})$$

$$\beta_\delta^{<n>} = \frac{g}{\rho_0} \sum_{m=1}^{n-1} \sum_{k=0}^{n-1-m} \frac{1}{m!} (\rho_x^{<k>}(x, 0, t))^{(m-1)} \zeta^{<l_1>} \dots \zeta^{<l_m>},$$

$$\forall l_1, \dots, l_m \text{ s.t. } \sum_{r=1}^m l_r = n - 1 - m - k, \quad (\text{density-induced return flow})$$

$$\chi^{<n>} = \sum_{m=1}^n \sum_{k=0}^{n-m} \frac{1}{m!} (A_\nu(x, 0, t) u_z^{<k>}(x, 0, t))^{(m)} \zeta^{<l_1>} \dots \zeta^{<l_m>},$$

$$\forall l_1, \dots, l_m \text{ s.t. } \sum_{r=1}^m l_r = n - m - k, \quad (\text{no-stress term})$$

$$\gamma^{<n>} = \sum_{m=1}^n \sum_{k=0}^{n-m} \frac{1}{m!} (u^{<k>}(x, 0, t))^{(m-1)} \zeta^{<l_1>} \dots \zeta^{<l_m>},$$

$$\forall l_1, \dots, l_m \text{ s.t. } \sum_{r=1}^m l_r = n - m - k, \quad (\text{tidal return flow})$$

$$\xi^{<n>} = \sum_{m=1}^n A_\nu^{<m>}(x, z, t) u_z^{<n-m>}(x, z, t). \quad (\text{mixing})$$

$$\xi_\chi^{<n>} = \sum_{m=1}^n \sum_{k=0}^{n-m} \sum_{i=1}^{n-m-k} \frac{1}{m!} (A_\nu^{<i>}(x, 0, t) u_z^{<k>}(x, 0, t))^{(m)} \zeta^{<l_1>} \dots \zeta^{<l_m>},$$

$$\forall l_1, \dots, l_m \text{ s.t. } \sum_{r=1}^m l_r = n - m - k - i, \quad (\text{mixing-no-stress interaction})$$

The higher-order equations are still all linear and every order is forced by solutions from the lower orders. As a result, the equations at each order are relatively easy to solve and the effects of different forcing mechanisms can be separated, even though the forcing terms themselves may become rather lengthy expressions. The second- and higher-order systems have six forcing terms, two of which are related to the density field. Density variations in our simulations only originate from a leading-order well-mixed salinity field, so that the two higher-order density related terms are not taken into account.

A2.2 Derivation of the turbulence closures

The base model uses a simple turbulence closure with two calibration parameters: the eddy viscosity A_ν and roughness parameter s_f . Most state-of-the-art 3D models on the other hand use the $k - \epsilon$ model. This model only needs one calibration parameter: the roughness height z_0 . While the single calibration parameter is preferable, the complex non-linear nature of the $k - \epsilon$ model conflicts with the principle of the idealised model, which requires that solutions are easily interpretable. In barotropic tidal flow cases, the $k - \epsilon$ model is still a complex non-linear differential equation model, but its forcing only has a single source the flow velocity. For such cases, it appears that one can express solutions of the $k - \epsilon$ model as simple algebraic functions of the velocity, depth and roughness.

In order to find these expressions, we use a complex 1D water column model with $k - \epsilon$ closure, see e.g. Dijkstra *et al.* (2016). This model is forced by range of depths H , depth-averaged M_2 tidal velocities U and

roughness values z_0 . We then search for the parameters in the simple base model closure A_ν and s_f that are needed to match the solution of the $k - \epsilon$ model for each of these forcing conditions. That means, we find functions $A_\nu = f(H, U, z_0)$ and $s_f = g(H, U, z_0)$ such that the simple closure matches the solution of the $k - \epsilon$ model. The solutions of both models are said to match if the total energy dissipation are the same in both the base model and in the $k - \epsilon$ model.

A2.2.1 M_2 tidal forcing and constant subtidal eddy viscosity

Based on scaling of the $k - \epsilon$ model and further theoretical analyses we assume that the functions f and g have the form

$$f, g = \gamma_1 U^{\gamma_2} (\kappa^{-2} C_D)^{\gamma_3/2} z_0^{\gamma_4} H^{\gamma_5},$$

where γ_i $i = 1, \dots, 5$ are yet to be determined, κ is the Von Kármán constant and where C_D is a drag coefficient as specified by Burchard *et al.* (2011) as

$$C_D = \kappa^2 \left[\left(1 + \frac{z_0}{H}\right) \ln \left(\frac{H}{z_0} + 1\right) - 1 \right]^{-2}.$$

When it is assumed that A_ν and s_f are time-independent, it follows from the fitting that approximately

$$A_\nu = 0.10U \left[\left(1 + \frac{z_0}{H}\right) \ln \left(\frac{H}{z_0} + 1\right) - 1 \right]^{-2} H, \quad (\text{A-7})$$

$$s_f = 0.22U \left[\left(1 + \frac{z_0}{H}\right) \ln \left(\frac{H}{z_0} + 1\right) - 1 \right]^{-2}. \quad (\text{A-8})$$

The quality of fit is presented in Figure 20. The crosses represent the matching A_ν and s_f for each of the 200 model settings (i.e. different H , U and z_0). The solid lines plot (A-7) and (A-8). There is a good correspondence between the separate experiments and the fit.

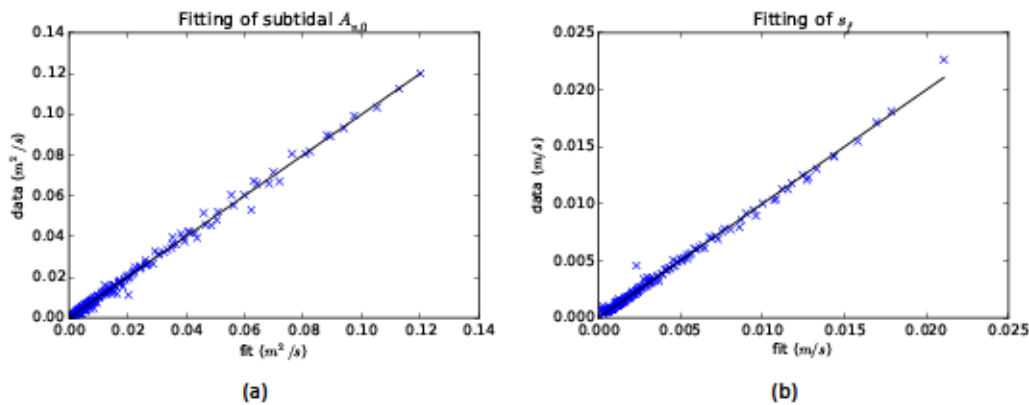


Figure 20 – Quality of fit for relation (A-7) (left) and (A-8) (right).

The base model takes a linear boundary condition and therefore chooses s_f as the parameter to prescribe externally (Section 3.1 and 3.2). This parameter is therefore either made constant or is at most allowed to vary with the depth. Rewriting and refitting (A-7) and (A-8) we can find an expression that relates A_ν to the prescribed value of s_f . This expression reads

$$A_\nu = 0.49s_f H. \quad (\text{A-9})$$

The matching of the simple base model turbulence closure and the $k-\epsilon$ model thus yields a simple expression relating A_ν to s_f . It is therefore a very efficient way of reducing the number of calibration parameters to one: the partial slip parameter s_f .

Alternatively to the linear boundary condition, one can assume a quadratic boundary condition, meaning that the bottom shear stress depends quadratically on the velocity (Section 3.3). This is the boundary condition used in most state-of-the-art 3D models. The quadratic boundary condition is provided directly by (A-7), (A-8) with z_0 or z_0/H as externally prescribed calibration parameter. To see this, note that the bottom boundary condition reads $\tau = \rho s_f u_{\text{bed}}$. According to (A-8) s_f depends on the velocity, so that we obtain a quadratic relation between the bed shear stress and the velocity. Experiments in the Scheldt model have shown that (A-8) is insensitive to whether it uses the depth-averaged velocity U or the near-bed velocity with a fixed conversion factor.

A2.2.2 Arbitrary forcing and time-varying eddy viscosity

The above equations describe the sub-tidal eddy viscosity and partial slip parameter for a single forced M_2 tidal component. This can be easily generalised. The typical time-scale required for attaining equilibrium conditions for turbulent mixing is much smaller than the tidal time-scale during most of the tidal cycle. It can therefore be assumed that the eddy viscosity just depends on the instantaneous velocity. One can therefore account for other tidal forcing components than the M_2 by considering the instantaneous velocity magnitude. We therefore replace the depth-averaged M_2 velocity amplitude U by the depth-averaged total instantaneous velocity magnitude $|u|$. $|u|$ describes a time-varying signal. The sub-tidal part of $|u|$ is related to U through

$$|u| = 0.64U.$$

This relation follows from a Chebyshev polynomial expansion of $|u|$. We thus rewrite (A-7) and (A-8) to

$$A_\nu = 0.16|u| \left[\left(1 + \frac{z_0}{H}\right) \ln \left(\frac{H}{z_0} + 1\right) - 1 \right]^{-2} H, \quad (\text{A-10})$$

$$s_f = 0.35|u| \left[\left(1 + \frac{z_0}{H}\right) \ln \left(\frac{H}{z_0} + 1\right) - 1 \right]^{-2}. \quad (\text{A-11})$$

This description has been verified by repeating the matching experiment with the $k-\epsilon$ model and (A-10), (A-11). The experiments now use a combined M_2 and sub-tidal flow or combined M_2 and M_4 flow. We define the ratios $\alpha = U_{\text{sub-tidal}}/U_{M_2}$ and $\beta = U_{M_4}/U_{M_2}$. Expression (A-10) provides a one-to-one relation between A_ν/U_{M_2} and α or β . Figure 21 shows the sub-tidal part of this relation for A_ν/U_{M_2} (solid line) compared to the results of the matching experiments. There is a large degree of scatter, especially for large α and β . Nevertheless the relation described by (A-10) fits the experiments fairly well. Similar fitting diagrams can be obtained for s_f , but are not shown here for brevity.

The scaling of the eddy viscosity with $|u|$ not only allows for an arbitrary forcing signal, but also provides a description of the time variation of the eddy viscosity. This time-dependent description is verified in Figure 22. This plots $A_{\nu M_2}/A_{\nu \text{sub-tidal}}$ and $A_{\nu M_4}/A_{\nu \text{sub-tidal}}$ plotted against α and β for both the relation of (A-10) and the matching experiments. This fit is generally quite accurate.

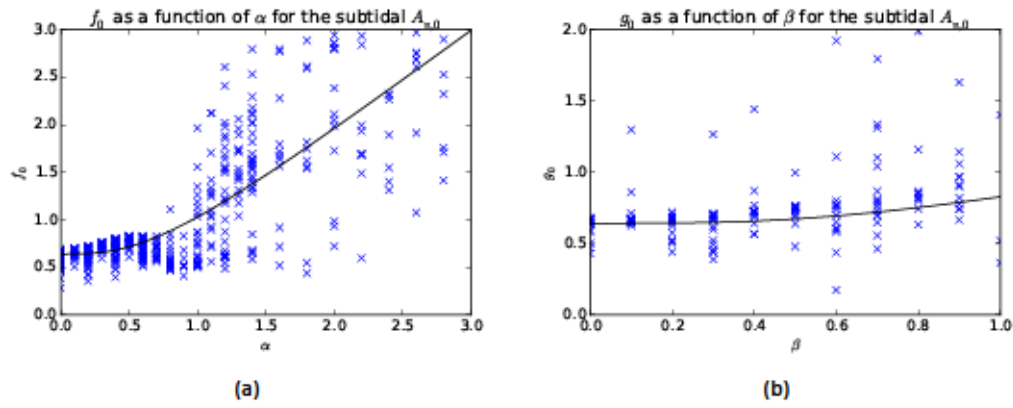


Figure 21 – Fitting of the sub-tidal part of $f_0(\alpha) = A_{\nu}/U_{M_2}$ and $g_0(\beta) = A_{\nu}/U_{M_2}$ as function of $\alpha = U_{\text{sub-tidal}}/U_{M_2}$ and $\beta = U_{M_4}/U_{M_2}$. The crosses show the results the matching experiments to the $k - \epsilon$ with combined M_2 and sub-tidal (a) and M_4 (b) flow. The solid lines are the relations given by (A-10).

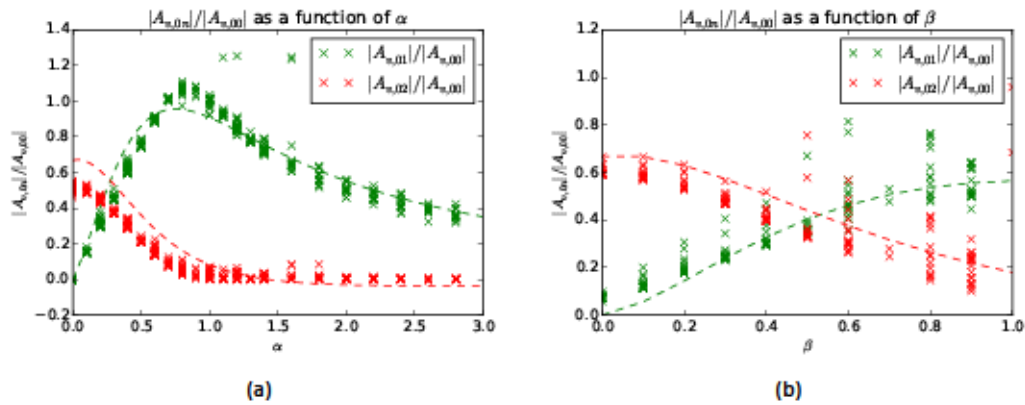


Figure 22 – Fitting of $A_{\nu M_2}/A_{\nu \text{sub-tidal}}$ (green) and $A_{\nu M_4}/A_{\nu \text{sub-tidal}}$ (red) as function of $\alpha = U_{\text{sub-tidal}}/U_{M_2}$ and $\beta = U_{M_4}/U_{M_2}$. The crosses show the results the matching experiments to the $k - \epsilon$ with combined M_2 and sub-tidal (a) and M_4 (b) flow. The dashed lines are the relations given by (A-10).

DEPARTMENT **MOBILITY & PUBLIC WORKS**
Flanders hydraulics Research

Berchemlei 115, 2140 Antwerp

T +32 (0)3 224 60 35

F +32 (0)3 224 60 36

waterbouwkundiglabo@vlaanderen.be

www.flandershydraulicsresearch.be